VISCOUS THREE-DIMENSIONAL FLOW SEPARATIONS FROM
HIGH-WING PROPELLER-TURBINE NACELLE MODELS

R.H. Wickens
Low Speed Aerodynamic Laboratory
National Aeronautical Establishment
National Research Council Canada
Ottawa, Canada K1A 0R6

SUMMARY

This paper describes an investigation of viscous three-dimensional flows on high-wing nacelle configurations which are typical of current commuter aircraft.

Flow visualization on two nacelle configurations was used to depict the viscous vortex separations in the underwing junction, the nacelle afterbody, and the wing upper surface over the central region. The surface shear stress patterns, although complex, were composed of combinations of elementary three-dimensional viscous flows and free vortices which stream downwind. A strong vortex flow was produced over the top of the wing by the use of leading edge extensions along the forward portion of the nacelle.

Observations were also made of the effects of a propeller slip-stream and the distortion of this propulsive flow by the mutual interference of the wing and nacelle.

SYMBOLS

A	aspect ratio $\frac{b^2}{S}$		V	flight speed
b, b_N	wing span, nacelle effective span		w	wake downwash
C_L	lift coefficient		y	spanwise location
C_D	drag coefficient		z	vertical location
e	wing efficiency factor		α	angle of attack
H	total pressure parameter $\dfrac{p_T - p_o}{\frac{1}{2} \rho V^2}$		α_{DW}	downwash angle (positive in negative lift direction)
p_T	total pressure		β_{SW}	sidewash angle (positive along starboard wing)
p_o	reference pressure		ϵ	wing streamtube deflection angle
S	wing area		θ	nacelle streamtube deflection angle

INTRODUCTION

This paper presents wind tunnel observations of various types of three-dimensional viscous flow separations on high-wing nacelle configurations which are representative of current propeller-turbine technology for commuter aircraft. These observations, in which flow visualization was used extensively, have dealt mainly with flows in the under-wing junction, along the top of the wing at high incidence, and on the nacelle afterbody. The models were unpowered, however, the effects of a propulsive streamtube, and slip-stream rotation were observed for certain cases.

Since most or all of the observed flows were of a three-dimensional vortical type, the surface shear stress patterns seen on the model surfaces reflected the presence of steady, rolled up vortex sheets which stream downwind. In addition, schematic representation of the various viscous singularities with which these complex flows can sometimes be represented, are also presented. In some cases it was also possible to do wake traverses in order to locate the regions of vorticity or separation.

Interest in this subject stems from Research and Development in Canada, and elsewhere, of a new generation of propeller-driven commuter class aircraft. The DeHavilland Dash-7 and Dash-8, now under development, are current examples. These aircraft exploit the advantages of the propeller-turbine propulsion system and reflect the most recent advances in aerodynamic design. Aerodynamic refinement of both the airframe and engine is necessary for efficient flight, and much information, both theoretical and experimental is being applied to the development of these new types of aircraft. One area which is of particular importance is the engine nacelle, and its design and placement on the wing so as to produce the optimum integration of lift and thrust. A typical aircraft development program requires large amounts of wind tunnel testing and analysis of data, leading to a final, satisfactory design; however, the present research program was undertaken to explore certain aspects of the aerodynamic flow over idealized wing-nacelle configurations (Ref. 7).

NACELLE AERODYNAMIC CHARACTERISTICS

In a wing-high configuration, typical of many current aircraft types, the main factors in the design and sizing of the nacelle, are the engine choice and placement, and the location, size and retraction mode of the main undercarriage. Having satisfied these requirements, the aerodynamicist must now shape the external contours to produce smooth flow, and minimum drag increments. His choices are narrow however; for example, the width of the nacelle and its cross-sectional shape, and also the afterbody length and shape,

DISCLAIMER NOTICE

UNCLASSIFIED
Technical
Report

DEFENSE
TECHNICAL
INFORMATION
CENTER

UNCLASSIFIED
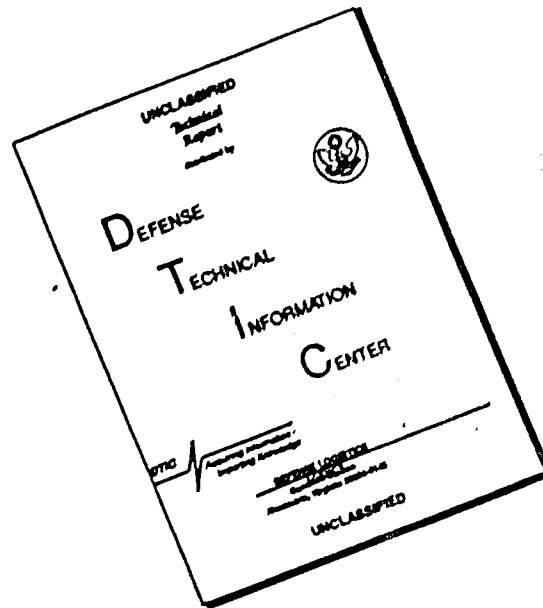
THIS DOCUMENT IS BEST
QUALITY AVAILABLE. THE COPY
FURNISHED TO DTIC CONTAINED
A SIGNIFICANT NUMBER OF
PAGES WHICH DO NOT
REPRODUCE LEGIBLY.

are important aerodynamic parameters but, these are essentially fixed by the retracted position of the main landing gear wheels, and the mode of efflux of the engine exhaust. The nacelle shape which evolves is usually somewhat functional, and may not represent the most efficient aerodynamic form, particularly in the vicinity of the wing, where interference flows are high, and separations are likely to occur.

Wing-nacelle interference and design has been the subject of a large amount of aerodynamic research and some of the more interesting and relevant conclusions have been summarized in References 1 to 10.

Early investigations on the subject showed that the measured drag of the wing-nacelle combination was considerably higher than the drag of the isolated wing, and that lift and lift distribution was also different, with a lift loss occurring over the nacelle. Assessment of complete aircraft configurations showed that for twin engined aircraft, the total nacelle drag could represent a large fraction of the total. It was these drag increments therefore, which were of concern to aircraft designers, and any improvements which might be gained, would be of significant benefit in the improvement of total aerodynamic efficiency.

The drag increment resulting from the addition of a nacelle to a wing is attributed to two main causes: the first results in an increase of overall induced drag due to the loss of lift. Part of this increase is also due to a reduced wing efficiency resulting from the non-uniform spanwise lift distribution over the nacelle. These distributions also result in the shedding of streamwise vorticity at the junction, which induces a non-uniform distribution of downwash along the wing span. These effects are different for different nacelle vertical locations. The centrally mounted nacelle has the smallest drag increment. The underslung nacelle results in a larger loss of lift and higher induced drag increment, however, these can be alleviated by adjustments to the wing and afterbody length. The effects of engine nacelle vertical placement on nacelle drag are shown in Figure 1.

A second type of interference drag arises in the expanding corners of the nacelle-wing junction near the wing trailing edge. Experience has shown that if the nacelle terminates at or before the trailing edge, separation is likely, with a resulting increase in drag. This type of flow is particularly severe with the underslung nacelle, as Figure 2(a) shows, but can be avoided by extending the nacelle beyond the wing, or by expanding the mid-section contours near the trailing edge, thus allowing the development of a steady, more gradual type of separation.

The significant regions of the wing-nacelle configuration where aerodynamic flows are important are the nose portion, particularly where the nacelle merges with the wing; the mid-section where interference velocities are high, and viscous separations are likely to occur; and the afterbody, from which steady three-dimensional separations should originate. The main physical parameters which affect the overall wing nacelle performance have been found to be:

1. wing vertical location,

2. position of nacelle maximum thickness, and

3. afterbody length behind the wing trailing edge.

To a lesser extent, nacelle cross-sectional shape is also important, particularly on the upper shoulder, just ahead of the wing leading edge junction (for high wing configurations).

If turbulent breakdown in the expanding corner is avoided by extending the afterbody rearward, the separation tends to be more gradual, and takes place along lines of confluence which fix the point of departure of the surface flows. Lines of confluence are defined as streamwise edges (virtual or fixed) along which fluids of differing velocities and flow direction meet. They are natural origins for vortex sheets and are a desirable element of flow detachment from slender streamwise configurations. The sketch (below) shows possible lines of confluence along the afterbody of a nacelle. This type of flow separation is the mechanism whereby the abrupt spanwise lift gradients produce the required wing-body vortices. It results in further vortex shedding but is, however, a satisfactory alternative to complete separation. In this regard, also, cross-section shape is important; a sharp edge would act as a natural line of confluence.
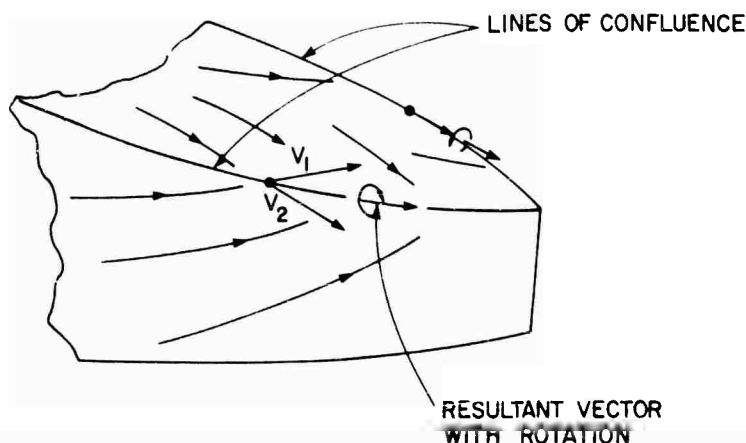
The importance of the efficiency of nacelle design on the overall drag and performance of an actual aircraft was illustrated graphically in the wartime research and development of the Douglas A26 attack bomber. This aircraft, one of the most successful of its type in World War II, and still flying today in the fire-bombing role, was initially troubled by poor performance as a result of unacceptably high nacelle drag. Investigation revealed that the two engine nacelles contributed over 30% to the total airplane drag. This drag was composed of cooling flow momentum loss, and drag due to the external contour. Of this latter drag, 75% was due to flow over the mid- and aft-portions of the nacelle, and 25% due to the flow over the engine cowling. By making suitable changes to the cowling contours, and by adjusting the shape and exiting cooling flow over the afterbody, the nacelle drag was reduced, with a corresponding increase in aerodynamic cleanness (Ref. 11).

The method used to assess the drag increments of the A-26 nacelles was a pitot rake, positioned downstream of the nacelle afterbody, which rotated about the nacelle reference line. The local drag coefficients so determined were found to be sensitive to the separation which was occurring on the nacelle afterbody, and the extent to which it was sensitive to upstream conditions (i.e. cooling exit mass flow).

LINES OF CONFLUENCE

RESULTANT VECTOR
WITH ROTATION

SKETCH (i)

WING-BODY INTERFERENCE

Drag and Vortex Wake

The physical nature of the inviscid interference between a wing and a fuselage or nacelle produces alterations in the forces (i.e. lift and drag), the pressure distribution, and the flow in the wake. Although the changes in lift may be small, the increases in drag can be significant and where nacelles are present and may account for a significant fraction of the total airplane drag.

The main inviscid interference effects on the wing have been shown to result in a slight decrease in lift over the centre section due to the reaction of the wing vortex system with the body, and a further increase in induced drag as a result of the abrupt changes in lift distribution across the span. The influence of the body may also extend outwards along the span of the wing, resulting in further small changes in lift and drag, due to the flow displacement effects of the wing thickness and fuselage volume.

The body (nominally a non-lifting system) will also experience inviscid interference effects which produce both lift and drag forces; and are due to an effective incidence change on both fore and aft regions resulting from the induced upwash and downwash field of the wing. Incremental pressure forces will also be present on the body as a result of its own shed vorticity, which has been carried over from the wing.

In all of these interactions, which are the most prominent in the junction itself, viscous flows are present in the form of skewed boundary layers on the body and three-dimensional attachment and separation regions in the junction and elsewhere. These viscous separations appear as concentrations of vorticity which stream downwind and make their own contribution to induced drag.

The alterations of lift and lift distribution, and the resulting induced drag are reflected, in classical inviscid vortex models, by distributions of lift which are considerably different from, for example, the elliptically loaded wing.

The wake which, at a later stage, rolls up to form trailing vortices, is an essential element of the entire flow; vortices will therefore be present even in an inviscid flow. Classical theory assumes that vortex sheets representing the wing, or combinations of a wing and body, extends into the wake long distances downwind of the configuration, to the so-called Trefftz plane, and that the down-wash resulting from this wake depends on the strength of the vorticity, and its distribution. Minimum drag for a given lift occurs when the wake vortex system, which has its own downward motion, moves without deformation, thus preserving the original shape of the cross-sectional flow as it left the lifting system. Thus the monoplane wing of minimum induced drag will have a drag polar of the form

$$C_{D_{i_W}} = \frac{C_L^2}{\pi A} \tag{1}$$

and a distribution of vorticity which is anti-symmetric and concentrated heavily near the wing tips.

The addition of a body changes both the downwash distribution and the drag polar.

Thus

$$C_{D_{i_{WB}}} = \frac{C_L^2}{\pi A \left[1 - \dfrac{R^2}{b^2}\right]^2} \tag{2}$$

and the induced drag is made somewhat higher by the addition of a wing at mid-height.

Moving the wing to the shoulder or high position changes both the spanwise load, and the drag, as shown by Pepper in Reference 14. Figure 3 shows, for the monoplane wing, and the wing body, with the wing at mid and high positions, the theoretical drag polars for minimum induced drag, and also the spanwise load distributions. The main difference between the mid and high wing location seems to be a reversal in the sign of the body lift, and hence the shed vorticity at the junction. The vortex sheets will roll up eventually to form concentrated vortex cores as shown. Figure 4 shows experimental spanwise lift distributions of wings on a cylindrical fuselage (Ref. 5).

A useful concept is the momentum streamtube (see sketch). This is an idealization which suggests that the trailing vortex wake and its circulating flows are contained within a descending cylindrical tube which streams downwind of the aircraft, and which contains all of the momentum associated with the production of lift. Thus for an aircraft flying at velocity V, the lift is

$$L = \rho V W_0 S_m \tag{3}$$

where W_0 is the bulk or average downward motion of the wake as a whole, and S_m is the cross-sectional area of the momentum stream-tube, for the monoplane wing, or for various wing-body configurations in which the vortex sheets have not rolled up; the addition of a body results in a diminished streamtube, and less lift for a given downwash. The classical flow models have assumed that the fuselage or afterbody is infinitely long, and retains its influence for ever. In fact flow will separate from the after body in the form of oblique rolled-up vortex sheets which, in an inviscid flow must occur along physical or viscous lines of confluence as noted in Sketch (i). The resulting wake model which must now represent the aerodynamic flow from the wing-body configuration will have to include free vortices which have been shed from the afterbody, and perhaps also other regions of the airframe. In this regard, some of the purely viscous flows, such as those in the under wing junction could be looked on as free vortex separations which comprise an equivalent inviscid flow model. The result of this altered distribution and formation of wake vorticity will affect not only lift and drag, but also the streamtube size and motion and the concept of minimum induced drag.

Junction Flow

The main results of wing-body interference have been shown to be related to changes in lift and induced drag, with vortex flows originating over the central portion. Some of these characteristics can be estimated using classical wing theory without any detailed knowledge of what is occurring at the wing-body junction itself. Local flows in the junction are important, however, and

frequently lead to overall effects such as separation, which further increase drag. Even where disorganized separation does not occur, three-dimensional boundary layer separation does, with shedding of additional streamwise vortices.

Since the interference flows are always generated in the junction between the wing and the body, the shaping of the intersection is important, and frequently results in elaborate fillets or contours which are meant to produce not only smooth flow, but also minimum pressure drag.

The main aerodynamic effects of wing-body interference at the junction can be divided into four main areas according to Reference 15.

(a) Displacement Effects

The displacement effect of wing-body interference has been shown to produce marked changes to the streamwise velocity distribution at the junction; these induced velocities result from the finite thickness of the wing, and the compound curvature of the intersection line. A symmetrical wing section at mid-height on a cylindrical body produces, along the junction, symmetrical velocity distributions, and results in no net lift on the combination. A similar, but asymmetric displacement effect occurs when the wing is set at an incidence relative to the body. In this case, a lift increment results which is related only to the asymmetry of the junction flows.

If the wing is lifted to the shoulder or high-wing location, the intersection lines are no longer symmetrical with respect to the cylinder. The resulting velocity distributions will also be asymmetric, and the wing-body junctions will thus generate lift, with the appropriate vorticity shed downstream.

(b) Lifting Effects

The lifting effects of wing-body interference as it alters total lift and lift distribution is fairly well described by lifting line theory and its extensions. In addition to these changes, however, velocity increments will also be induced along the junction intersection lines due to the vorticity distributions on both the wing and the body.

The placement of a lifting wing on a cylindrical body set at zero incidence, for example, produces alterations in the wing spanwise vorticity and a continuation of this vorticity over the body width. Thus velocity increments are produced on both the wing and the body as a result of their proximity.

Detailed calculations of such flows are discussed in References 15, 16 and 17 and these indicate that both chordwise and spanwise load distribution, and hence local velocities are changed considerably in the vicinity of the junction and beyond. This requires that, for the isolated wing loading to be maintained everywhere, the wing must be cambered and twisted. This type of wing warping is also alluded to by Hoerner (Ref. 3) and Reference 1, in relation to the induced drag of underslung nacelles. By adjusting the local wing loading at the nacelle location using a trailing edge flap, the lift increment of the configuration may be to zero with a corresponding reduction of induced drag.

If the body is also lifting, and the carry-over of vorticity from the wing implies this, then there will be a further interaction at the wing. If there is body incidence, then the resulting upwash at the wing will increase the loading generally, with corresponding increases in the velocity increments in the junction.

(c) Non-Symmetrical Wing Locations

The overall changes to lift and drag when the wing is lifted from mid- to shoulder height on a cylindrical body can be seen in the drag polars of Figures 3 and 4. The flow at the junction, due to both displacement and lift effects is also altered considerably. The displacement flows are now asymmetric, and result in lift, independent of incidence (Ref. 15).

Induced velocity increments due to lift are also changed in character when the wing is off-centre. The wing vorticity is carried over on to the body and within it in a much more complex way; the resulting velocity increments, for example, in the underwing junction, are in the present state of the art, of uncertain magnitude and accuracy (Ref. 15).

Measurement of wing lift distributions, such as those indicated by Figure 4 suggests that there are large concentrations of pressure near the wing leading edge junction. Figure 5 taken from Reference 8 shows pressure isobars on the upper surface of a high-wing body configuration at an angle of attack of 2.5°. The concentration of isobars near the leading edge junction indicates a local change of both lift and leading edge suction.

(d) Viscous Effects

The viscous flows result in a gradual development of three-dimensional boundary layers on the nacelle and wing. Boundary layer separation occurs along oblique separation lines in the junction and elsewhere, with trailing vortices shed downstream. These flows are particularly prominent on the nacelle, which has a short after body.

The assessment of viscous effects are mainly undeveloped, but are considered to be of equal (if not of more) importance in contributing to wing-body interference. Whereas lift interference can be calculated fairly accurately under some conditions, drag interference cannot be, and an inspection of any of the viscous flows which appear in the wing-body junctions or elsewhere shows why (Fig. 13).

The complexity of these flows precludes any accurate estimate of drag, however, the existence of steady rolled-up vortex sheets suggests that it may be attributable to induced effects. It is also noteworthy that the surface shear stress patterns (as in Fig. 24) of the viscous attachment regions in the junction and aft of the trailing edge, bear a resemblance to a source-like flow in which momentum is related to drag. Thus viscous losses arising from junction flows might be contained within a streamtube whose dimensions roughly encompass the frictional shear stress regions as estimated from surface observations and would be related the vortex flows within them.

a) JUNCTION SEPARATIONS
ONLY

b) JUNCTION AND FOREBODY
SEPARATIONS
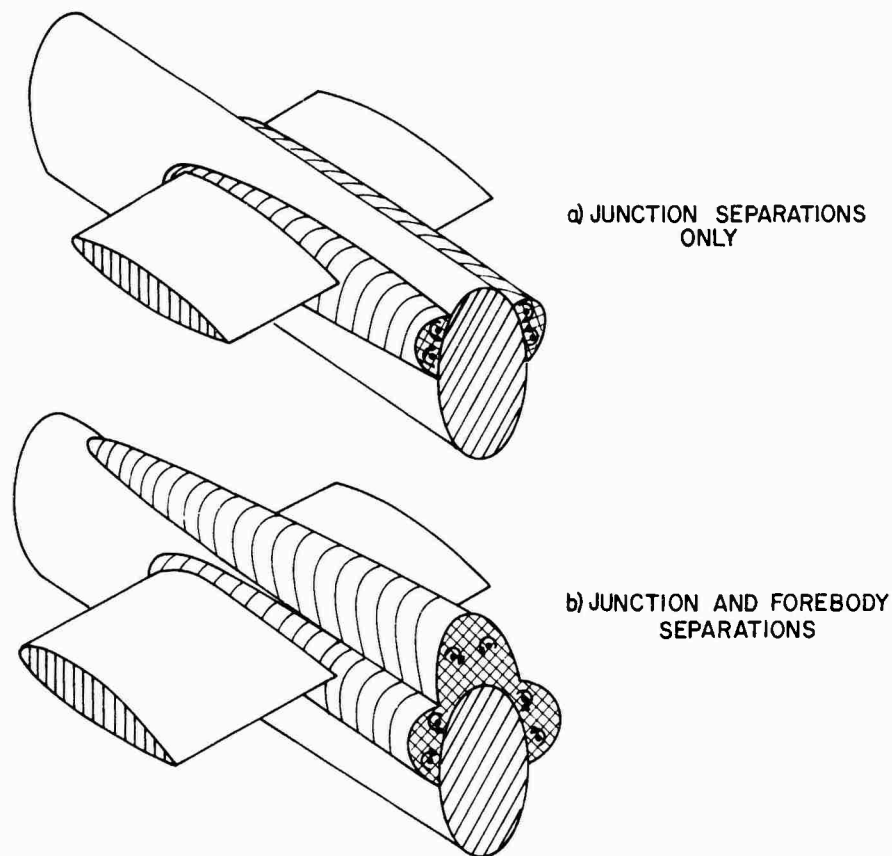
SKETCH (ii)

The nature and complexity of the viscous separations along the wing-body junction were also investigated in the NAE water tunnel using models which are typical of current nacelle designs. These flows are shown in Figure 6 and although at a very low Reynolds number they correspond very closely with larger scale tests, and demonstrate the complex nature of the viscous effects near the wing root leading edge.
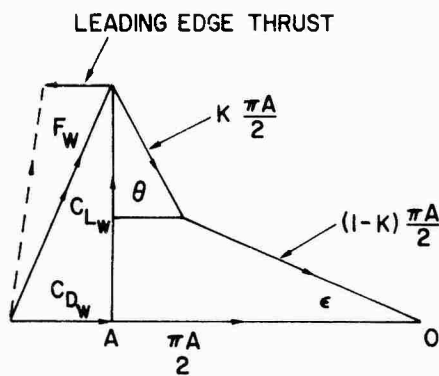
Propulsive Effects

An important element of the flow over the wing-nacelle configuration relates to the propulsive streamtube produced by a propeller. The slipstream is composed of mainly axial and rotational fluid motion induced by a helical vortex system which leaves the blades, and interacts with the wing and body. This interaction produces further changes in lift and drag, and is an essential design feature of aircraft designed for the STOL mode. Its effect is favourable in that it results in an altered span load distribution, reduced induced drag, and a favourable environment for the wing boundary layer outside the slipstream.

The aerodynamic loading on both the wing and the body, will also change, as will the junction flows and also the configuration of the wake vortex sheets. The propeller slipstream, initially cylindrical, will undergo considerable deformation, particularly on the under side of the wing, and will gradually merge with the wake vortex system of the nacelle. The flow downwind of the wing-nacelle will therefore be composed of both propulsive and vortical elements.

The propeller slipstream, particularly the flow rotation component, will have a major effect on the flow and pressure distribution at the wing leading edge junction and the concentration of vorticity which normally appears on a high-wing configuration (Fig. 5) will be enhanced on the up-going blade side, due to the local increase of incidence, and reduced on the down-going blade side, resulting in an overall increase of leading edge suction, and an asymmetric distribution of pressure. If LEX are installed, with vortex separations leaving the streamwise edges, then slipstream rotation may produce an asymmetric three-dimensional separation with free vortices of unequal strength streaming downwind.

The design of leading edge extensions for propeller-driven aircraft must conciliate the conflicting requirements at the leading edge for smooth flow and the development of maximum suction in the cruise and climb mode, with steady separated flow and vortex-induced lift during the landing approach.

The overall effect of a propulsive flow on a wing or wing-body can be assessed by the use of a simple two-stream momentum model as described in Reference 18. In this idealization, part of the lift and all of the thrust is derived by deflecting and energizing a streamtube of air which passes through the propulsion system. The remainder of the lift is generated by a wing or wing-body which is considered to deflect downward, a second streamtube. The sketch shown below is the vector diagram of the two-stream model.

LEADING EDGE THRUST

SKETCH (iii)

The vector OA is the approaching streamtube momentum of magnitude $\frac{\pi A}{2}$. If the wing or wing-body is unpowered, then the flow leaves the wing at downwash angle ϵ. If power is applied over part of the wing, it is assumed that a certain fraction of the department momentum $\frac{K\pi A}{2}$ leaves the wing at angle θ, while the remainder $(1 - K)\frac{\pi A}{2}$ leaves at angle ϵ. Thus the effective span of the powered lift streamtube is proportional to $\sqrt{K}$.

The vector F_w is the resultant force acting on the airframe, having components C_{L_W} and C_{D_W}. If the wing is immersed in a propeller slipstream, then the rotational components of the propulsive flow may enhance the leading edge suction on either side of the nacelle, resulting in a thrust or reduction of induced drag. The vector $\frac{RK\pi A}{2}(1 - \cos\theta)$ is that fraction of nacelle induced drag which is recovered at the leading edge.

Lift and drag coefficients (for small angles) are:

$$C_{L_W} = \left(\frac{\pi A}{2}\right) \epsilon \left[(1 - K) + \frac{K\theta}{\epsilon}\right] \tag{4}$$

$$C_{D_W} = \left(\frac{\pi A}{4}\right) \epsilon^2 \left[(1 - K) + K(1 - R)\left(\frac{\theta}{\epsilon}\right)^2\right] \tag{5}$$

This leads to a drag polar of the form:

$$C_{D_W} = \frac{(1 - K) + K(1 - R)\left(\frac{\theta}{\epsilon}\right)^2}{\left[(1 - K) + K\frac{\theta}{\epsilon}\right]^2} \cdot \left(\frac{C_{L_W}^2}{\pi e A}\right) \tag{6}$$

and wing efficiency factor is:

$$e = \frac{\left[(1 - K) + K\frac{\theta}{\epsilon}\right]^2}{(1 - K) + K(1 - R)\left(\frac{\theta}{\epsilon}\right)^2} \tag{7}$$

Figure 7 shows e plotted against the ratio $\left(\frac{bn}{b}\right)$ for values of $\left(\frac{\theta}{\epsilon}\right)$ of 2, corresponding to a positive nacelle lift increment, and 0.5, corresponding to a negative nacelle lift increment. The effect of a 10% recovery of leading edge thrust is also shown.

These results show that when the combination of propulsive and interference effects are distributed uniformly across the span, $\left(\frac{\theta}{\epsilon} = 1\right)$, then wing efficiency factor is a maximum, and equal to unity. If the angles differ markedly, then e decreases, and as Figure 7(b) shows, reaches a minimum when the spanwise disturbance covers about 60% of the span. It appears, therefore, for high wing efficiency factors, that any spanwise disturbances should cover either a very small portion of the wing span, or a very large portion. In this regard, the negative lift increments produced by the presence of an unpowered nacelle result in a lower loss of wing efficiency than positive increments produced by powered lift. The effect of a leading edge thrust recovery factor R results in an increase of wing efficiency factor in both cases.

The two-stream flow model has assumed that all of the momentum associated with both propulsive and wing-body interactive effects are contained within the propulsive streamtube. Viscous effects, which are also encompassed within this region contribute indirectly in that they represent a portion of the flow which may be deflected with the general flow over the nacelle. They are, however, non-productive, resulting in a loss of momentum, and, specifically a loss of leading edge suction at the wing-nacelle junction.

WIND TUNNEL MODELS

The nacelles were mounted in the underwing position on a rectangular planform reflection plane model. The wing airfoil was the NACA 0015 and had an equivalent aspect ratio of 6.58, Figure 8 is a general arrangement showing the basic dimensions. The model was attached to the wind tunnel balance for the purpose of measuring lift and drag.

The basic proportions of the nacelles, relative to the wing chord, were chosen to be similar to those under consideration for commuter aircraft design studies. Two basic thickness distributions and cross-sections were chosen. The first (N-1) was based on the NACA standard body as described in Reference 8. A variation of this form, with the maximum thickness pushed back to 60% of wing chord, was tested since the data of Reference 1 indicated a favourable result when maximum thickness is close to the wing trailing edge. The afterbody terminated 0.65 wing chords behind the trailing edge in an ogival contour.

The second model (N-2) was elliptical in cross section and of more slender configuration. The fore and aft body lengths extend 1.2 and 0.8 wing chords beyond the wing leading and trailing edges; the after body terminated in a vertical trailing edge. Figure 8 shows the basic form of the two nacelles with relevant dimensions noted. On nacelle N-2, leading edge extensions (LEX) were fitted in order to encourage the formation of vortices over the top of the wing.

WIND TUNNEL TEST PROGRAM

Balance Data

Force measurements were made at a tunnel dynamic pressure of 40 psf ($R_e = 1.2 \times 10^6$). The model was rolled through an angular range which brought the wing beyond stall, with lift, drag and moment recorded.

Lift and drag coefficients for the two configurations, including the isolated wing are presented in Figures 9(a) and 9(b). The main effect of adding a nacelle is to decrease $C_{L_{max}}$ and stalling angle. The lift and drag characteristics for the isolated wing in the linear range of lift implies a wing efficiency factor $e = 0.75$. The addition of a nacelle decreases e slightly, to a value of 0.6. Figure 10 shows, for nacelle N-3, the effects of adding the LEX, on maximum lift, and drag. There is evidently an increase in lift and a small increase in lift slope due to the presence of free vortices shed from the LEX. This is accompanied by a decrease in L/D at angles greater than 10 degrees.

Model pitching moments are also changed by the presence of a nacelle as seen in Figures 9 and 10. With the short nacelle (N-1) the pitching moment destabilizing (nose up); however Cm reverses sign over the α range from 4 to 14 degrees on the slender nacelle (N-2). The addition of leading edge extensions on nacelle N-2 reverses the sign of the pitching moment from nose down to nose up.

Flow Visualization

The medium for flow visualization was Titanium Dioxide suspended in a light machine oil. When illuminated by a strong light source, the TiO_2 gave off a brilliant reflection, and the properties of the suspension were such that spreading took place in the form of streamwise ligaments when exposed to the frictional layer on the model surfaces.

Water tunnel flow visualization was done at very low Reynolds number using coherent filaments of Flourescien, a commercial dye. In some instances at higher Reynolds number, a suspension of Aluminum particles enabled vortex flow fields to be visualized.

Downwind Flow Surveys -- Powered Models

Downwind flow surveys using pitot tubes, or five-hole yawmeters were made behind two powered wing nacelle models. The first was a powered version of nacelle N-2 (Fig. 8); the power effects resulted in both axial and rotational velocity components over the nacelle and wing.

More extensive measurements (i.e. velocities, total pressure, flow direction) using five-hole probes were made behind a large-scale powered wing-nacelle model which was under investigation by DeHavilland Canada. The proportions of this model were, in general, similar to nacelle N-2.

The purpose of these flow surveys was to locate localized regions of separation, and centres of vortex activity, and also to explore the deformed slipstream downwind of the model.

Classification of Three-Dimensional Viscous Flows

Three-dimensional viscous flows, such as those depicted by the photographs of surface streamlines shown in this paper, appear to be of a very complex nature, as they reflect the combined action of skewed, separating boundary layers, and the action of rolled up vortex sheets lying just above the surface. These apparent complexities, however, can be separated into various combinations of relatively few simple singular flows, which act on the wetted surfaces, and satisfactorily describe the action of viscous separations and attachment. The anatomy of these singular flows has been thoroughly described in References 19 and 20. They are seen to occur regularly in the skin friction patterns of all three-dimensional attached and separated viscous flows, and are related either to regions of attachment or of separation on the body. They are classified schematically, as in Figure 11.

The nodal point of attachment is shown in Figure 11(a) — the oncoming flow impinges on the nose of the body at a single point, and the surface streamlines radiate outward and rearward toward the leeward side.

If two adjacent nodes of attachment occur, as on the blunt surface of a windshield the streamlines divide between them and are redirected, by means of a saddle point, on either side of the line of symmetry.

If the onset flow impinges obliquely on a slender configuration, or along intersecting surfaces, then attachment is not at a single point or node, but along an oblique line of attachment. This type of flow can be seen along the windward surface of the nacelle (Fig. 12) or along the under wing junctions. Surface fluid always flows away from an oblique line of attachment toward separation lines, or the general flow.

Figure 11(d) and (e) shows various aspects of three-dimensional separation. Figure 3 is a nodal point of separation which would permit closure of the streamlines in an ideal flow. This does not occur in practice as other modes of separation occur on the aft portions of a body.

The focus of separation, (Fig. 11(d)) is characterized as a surface flow in which the streamlines spiral inward toward a clearly defined centre. A vortex core rises from this centre, and streams downwind. The flow at the spiral focus has been interpreted (Ref. 19) as the termination point of bound vorticity which leaves the surface in a single concentrated filament. The spiral foci are clearly evident on the wing-nacelle models when separation occurs (Fig. 26) and on the windward side of a leading edge strake (Fig. 17). These flows are considered to be undesirable since they tend to detach randomly from the surface and are associated with buffetting and periodic flow separation.

Figure 11(e) shows an oblique line of separation, a flow which is characteristic of separation from slender wings and bodies. Boundary layer fluid approaches the line of confluence from both sides, and separates as a thin sheet which rolls up above it. If the vortex is strong enough, the surface shear stress lines may exhibit a point of inflexion in their curvatures. The attachment line depicted in Figure 11(e) along the plane of symmetry represents the presence of fluid which has been brought down on to the surface as a result of vortex action.

WING-NACELLE VISCOUS FLOW SEPARATIONS

This section presents observations on the main characteristics of the various types of three-dimensional flow separations which occurred on the wing-nacelle junction region. The comments are supported by photographs and interpretation of the surface shear stress patterns in the context of the elementary viscous singular flows described before. The interpretation of the surface flows and their synthesis into equivalent vortex flow models are somewhat subjective, and, as Reference 21 points out, notoriously ambiguous and open to question. Nevertheless, it is hoped that a clearer understanding of the steady separated vortex flows over the nacelle will result, and that this work may be useful as a point of departure for a more complete understanding of the aerodynamic flow over wing-nacelle configurations.

Attachment Flows

Regions of flow attachment are shown on the windward portions of nacelle N-2 at an angle of attack of 21 degrees (Fig. 12). In this flow, the node of attachment, at the nose of the spinner, develops into an oblique line of attachment along the ventral surface of the nacelle, and from which fluid flows along the sides of the nacelle, toward the wing junction and afterbody. The lateral deflection of the flow on either side of this line, particularly at the nose is severe, but diminishes over the mid section and upswept afterbody.

Leading Edge Junction - No LEX

The flow near the leading edge, along the wing root junction, as depicted in the water tunnel photographs of Figure 6, represents the main viscous interaction between the nacelle and the wing. As these illustrations show, for a normal leading edge, the stagnation region between the wing and nacelle produces a sudden local separation which has resulted in a horseshoe-type vortex which wraps itself around the wing contour, and whose trailing arms stream downwind.

The surface shear stress pattern of Figure 13 shows, at a Reynolds number of 1.2 x 10⁶, a variety of discrete separation and attachment regions which are concentrated within a fairly narrow band along the underside of the wing. Details of this surface flow for nacelle N-2 are shown for angles of attack of 0,8 and 16 degrees.

On the basis of these flow patterns, it is possible to identify both primary and secondary oblique separation lines, nodes of attachment between them, and oblique lines of attachment lying along the sides of the nacelle. In the case of α = 16°, it is also possible to identify the stagnation streamline which separates fluid which flows over the top of the wing, from that which traverses the length of the nacelle.

A schematic interpretation of the junction flow shows the probable origin and behaviour of the vortex filaments shed from the junction (Fig. 14). This vortex appears to remain coherent underneath the wing, but is apparently embedded in the boundary layer flow on the upper surface or, since there is little reason for its existence, probably dies out. No trace of it was discernible on the nacelle afterbody. The secondary vortex, although visible in the underwing junction, has apparently merged with the primary vortex on the wing upper surface.

Leading Edge Junction with Leading Edge Extensions (LEX)

In the normal wing junction geometry, the wing meets the nacelle squarely, the only relief afforded by the body curvature on the upper surface. The junction vortex is thus formed abruptly and the resulting flow is as that shown in Figure 6(e). In order to encourage a more gradual formation in the vortex and to change the stalling characteristics a leading edge strake or extension was placed on the top of the nacelle ahead of the wing leading edge. The strake configuration and dimensions are shown in Figure 8.

With this device fitted, free vorticity is shed along the streamwise edges as flow coming up from the ventral attachment line separates along the top of the nacelle. The vortex sheets roll up above the wing, producing downwash in the place of symmetry, and increased lift. At high incidences, these vortices become part of the separated, but steady flow on the wing upper surface.

The junction vortex system which originates on the strake windward edge exists, but exhibits an altered behaviour. The flow on the windward side of the strake, upwind of the stagnation streamline, leaves the swept edge, and rolls up immediately into a strong free vortex above the nacelle. Flow on the nacelle upper surface also flows toward this separation line.

Flow downwind of the stagnation streamline is directed along and underneath the nacelle as before. Between these two flows, on the strake itself, is a region of three-dimensional separation and attachment, similar to the normal leading edge situation, in which surface fluid flows along the underwing junction in one direction, and toward the swept edge of the strake in the other, a prominent node of attachment lies at the wing-nacelle junction. A primary vortex sheet leaves the separation line and, on the underside of the wing, gradually develops and rolls up underneath the wing as before. There is an impression that the junction vortex produced this way is somewhat weaker than its normal counterpart. The flow patterns, especially in the attachment region along the underwing junction do not exhibit a particularly strong three-dimensional effect. A secondary vortex separation is also present, and behaves in a similar fashion to the primary flow.

The other half of this horseshoe vortex is directed across the half-span of the strake, and leaves the edge together with flow from the attachment region, to roll up and become merged with the free vortex which by now is well developed above the nacelle surface.

The development of the strake vortex flow appears in the surface shear stress patterns of Figure 15 and schematically in Figure 16.

There appears to be two ways in which the underwing vortex can develop. If the strake is suitably blended into the wing-nacelle junction, then the gradual separation process produces the attachment region on the windward surface, with vortices gradually developing as shown. If the strake is not properly designed, or simply consists of a thin plate normal to the nacelle surface, the stagnant fluid in the re-entrant corner appears to encourage the formation of a spiral focus, which acts as the origin of the underwind vortex (Fig. 17). This flow situation is undesirable because of its unsteady nat re.

The photographs and schematic diagrams of Figures 15 and 16 show the two possible modes of flow and separation with the strake fitted.

Flow on the Wing-Nacelle Upper Surface — No LEX

The flow on the upper surface of the nacelle at angles below stall is composed mainly of fluid which has left the ventral attachment region, flowed around the sides of the nacelle and along the top of the wing. In addition, there are narrow regions of three-dimensional flow induced by each junction vortex as it streams over the top of the wing. The behaviour of the flow on the wing/nacelle upper surface is critically affected by angle of attack. The three-dimensional effects induced by the junction vortices become more prominent, and the unseparated flow between them is subject to rapid changes in velocity as judged from the streamline patterns of Figure 18 for nacelle N-1.

As incidence increases, new separation lines emerge, on the top of the nacelle at the wing leading edge. These evidently result from detachment of fluid along the top of the nacelle which does not enter the junction separation region. The vortices which are shed are depicted in the sketch as rotating inward, and will be the beginnings of the full-scale wing upper surface vortex flows which are prominent near and after stall. The junction vortex filaments which search away from these new vortices are probably eventually swallowed, and would not appear downstream. If flow separation is premature then the breakdown of the wing boundary layers produce undesirable aerodynamic characteristics, and this is reflected in both the surface shear stress patterns and the lift and drag characteristics.

With a more slender nacelle (N-2), as stall develops, it is possible to see more easily what happens to the junction vortex on the upper surface. Figures 19(a), (b), (c) show, for a wing with a normal leading edge, the gradual development of three-dimensional separation leading to prominent but unstable vortex flows for angles of attack of 0, 16 and 30 degrees. The schematic interpretation of this process indicates that the junction separation lines may terminate at spiral foci on the wing upper surface near the leading edge. Separation appears to occur as a result of vortex filaments leaving these foci, but also from weak oblique separation lines which traverse the wing chord. These two flow separations presumably merge with one another.

Flow on the Wing Upper Surface — LEX Installed

With a strake fitted, the upper surface flow is dominated mainly by the vortices shed from its free edges, even at moderate angles of attack. Figure 21 shows for nacelle N-2 the upper surface flows at angles of attack of 0, 8 and 16 degrees.

The flow is now more stable, and, in comparison with no LEX, at 8 degrees, composed entirely of three-dimensional flow over the centre section. The separation lines, which commence along the streamwise edges of the strake, continue across the wing chord to the trailing edge and begin to form the main vortex system which, at high lift coefficients, keeps the flow attached on the centre section. In this way the classical decrement of loading over the centre portion of a wing-body may have been "filled in" by the action of a favorable viscous separation. The lift curves of Figure 10(a) indicate a slight increase in lift.

The flow in the vicinity of these separation lines, particularly in the interior region, is notably three-dimensional, and exhibits many of the characteristics of the shear stress patterns seen on slender delta wings. At higher angles of attack ($\alpha > 16°$) outboard of the main separation lines, fluid is drawn to both primary and secondary separation lines which originate well beyond the physical dimensions of the nacelle. The schematic diagram of Figure 22(a) shows the main features of the vortex flow over the top of the wing, induced by leading edge extensions. Attachment takes place along the line of symmetry for $\alpha = 8°$. At higher angles of attack, when the vortex flows are stronger, two attachment lines lie on either side of the plane of symmetry.

There appears to be an alternate configuration of the upper surface vortex sheets which may occur at low angles of attack. In this situation, shown in Figure 23 the separation line which originates on the streamwise edge of the LEX does not continue on to the wing. Rather, the vortex sheet may detach at the wing LEX junction, and both ends roll up, resulting in the formation of double branched cores over the wing. The resulting flow disturbance on the wing may be small. This conjecture has not, so far, been supported by direct observation, and as wing incidence increases; there is a greater likely hood of the vortex sheet "sticking" to the wing. The junction vortex, which does not appear on the wing upper surface with LEX installed, presumably rolls up with the free vortex sheet.

Afterbody Attachment and Separation

Another region where significant separation and reattachment occurs is just aft of the wing trailing edges, on either side of the nacelle afterbody. These attachment regions as seen in Figure 24 for nacelles N-2 and N-3 are slender formations of three-dimensional flow with a prominent node of attachment at the nose. Fluid apparently flows from the oblique attachment line located in the center of these regions to separation lines around the periphery. The sense of the shed vortices is uncertain; Reference 21 discusses a similar flow at the trailing edge of a two-dimensional wing-plate configuration at comparable Reynolds numbers. These trailing edge separation patterns were attributed to a continuation of the secondary vortex flows generated in the junction; thus the flow in the attachment region was weak, and the sense of the free vorticity was opposite to the primary junction vortices.

In the present situation, aft of the wing-nacelle, the reverse is true, in the author's opinion, since the attachment flows appear to be strong, and to suggest vorticity which is rotating in the same sense as the junction vortices.

The size of this attachment region appears to depend on the shape of the nacelle afterbody; the wider, more blunt-ended NACA nacelle (N-1) has significantly larger regions of disturbance, than does the more slender configuration (N-2). A schematic interpretation of the flow on the nacelle afterbodies is shown in Figure 25.

REYNOLDS NUMBER EFFECTS

The present tests were done at a fairly low Reynolds numbers, ranging from about 5000 in the water tunnel to 1.2×10^6 in the wind tunnel. The structure of the wing root junction flow contains not only primary vortices, but also secondary, and in some

instances, tertiary separations along the sides of the nacelle. This multiple vortex shedding tends to be a characteristic of three-dimensional protuberance flows at these low Reynolds numbers, but is found not to occur at the higher Reynolds numbers which correspond to full-scale flight. Thus in attempting to describe the staggering multiplicity of vortices which stream downwind of a wing-nacelle configuration, it should only be necessary to count the primary separations. The sketches in Figure 26 depict various combinations of vortices which should appear in cross flow planes downwind under different conditions of flight. If the upper surface flow is unseparated, with a normal leading edge, then a total of eight primary vortex cores stream from the junctions, and afterbody separations. If a LEX is installed, with vortices streaming from the swept edges, then additional vortices will appear above the wing bringing the vortex. If the propulsive streamtube also deforms and rolls up, as the wake survey's tend to suggest, then additional areas of vorticity will be present in the flow downwind.

EFFECTS OF A PROPELLER SLIPSTREAM

The effects of a propulsive streamtube, and slipstream rotation are shown in Figures 27 to 30.

The powered version of nacelle N-2 did not produce high thrust levels; the average value of the pressure rise behind the propeller corresponded to a total pressure coefficient $C_p = 1.1$. This did not result in large velocity increments, however, the slipstream rotation was quite large, and yawmeter measurements indicated a value of about 10 degrees at a radius corresponding to the maximum nacelle width.

Flow visualization indicated some of the changes caused by the slipstream. With LEX installed on nacelle N-2, at low model incidence ($\alpha = 4°$), the flow on the ventral surface was seen to reflect slipstream rotation, and the flow pattern on the wing upper surface was slightly skewed toward the downgoing (outer wing) blade side. At very high angles of attack, with separated flows over the wing surface, the slipstream tends to encourage a more symmetric flow formation that would otherwise occur. In the middle ranges of α there appeared to be no noticeable alteration in the flow patterns due to slipstream effects.

With a normal leading edge (no LEX) the slipstream rotation effects are present for angles of attack only greater than 16 degrees, in that the upper surface flow patterns were slightly skewed toward the outer wing.

A total pressure survey was also done behind the powered and unpowered versions of nacelle N-2 (LEX on), at mid chord, on the wing upper surface. At 16 degrees, (unpowered, Fig. 27(a)), just before stall, the isobars indicate the presence of two stable vortices, spaced 1/3 chord apart, and lying about 1/10 chord above the wing surface. At 20 degrees, well beyond $C_{l_{max}}$, the starboard or inner vortex has become incoherent with flow breakdown occurring over the wing (Fig. 27(c)).

Isobars for the powered nacelle, at angles of attack of 16 and 20 degrees are presented in Figure 27(b, and (d). Slipstream effects do not appear to produce any important changes in the appearance of the flow for these angles.

Further explorations of the nacelle-wing wake were made using five-hole yawmeters behind a more heavily loaded configuration. The model was similar in its proportions to nacelle N-2 although not of the same design. The test conditions were appropriate to a climb configuration, with a fairly high thrust coefficient, and flaps set at 15 degrees.

The measurement plane was three chords behind the aerodynamic centre, and the quantities shown in Figure 28 are sidewash and downwash angles. β_{sw}, α_{ow}, and total pressure H (Fig. 29).

Observations in the cross-flow plane showed that the propulsive streamtube of the propeller was grossly deformed by the mutual effects of the wing and the nacelle. In addition, as a result of viscous separation in the wing-body junction, and the roll-up of the propulsive streamtube, regions of concentrated vorticity were present in the flow.

The total pressure contours of Figure 29 trace out the configuration of the deformed slipstream, which in this case tends to form an "inverted T", a configuration which as been observed before (Ref. 22). The slipstream flowing over the top of the wing is evidently contracting, while that flowing over the bottom contains most of the really high pressure levels, and appears to be spreading laterally beyond the physical dimensions of the propeller.

It was difficult to identify precisely, any regions of vorticity, however, the downwash contours suggest vortex-like activity below the wing on the up-going blade side. The sense of rotation of the cross-flow appears to be clockwise, viewed from the rear, and is consistent with a vortex shed from the port wing body junction. Similarly, the sidewash angle contours indicate a similar type of rotation, also originating from the port side.

CONCLUSIONS

The aim of this paper has been to summarize some of the important problems in the integration of a wing and nacelle, for turbo-propeller aircraft, and to emphasize in particular, the viscous interations which occur.

The nacelle models were sized to represent current practice, and were mounted on a half-wing of aspect ratio approximately six. Balance measurements demonstrated the characteristic decrease of lift and increase in drag which occurs when an underslung nacelle is added to a wing. The addition of leading edge extensions (LEX) resulted in a slightly improved lift slope, higher $C_{l_{max}}$, and a gentle stall.

Flow visualization showed that steady three-dimensional separations with rolled-up vortex sheets played an important role in the development of good aerodynamic flow over the wing-nacelle configuration. These vertical flows occurred in three main regions of the nacelle; firstly at the wing-nacelle junction where a horse-shoe shaped separation line sweeps along the underwing junction, and over the top of the wing. A vortex sheet is shed from this line, and rolls up gradually along the length of the nacelle, bringing the oncoming fluid into the intersection. Secondary separations may also occur.

The second important region of three-dimensional separation and attachment lies aft of the wing trailing edge, on either side of the nacelle upper surface plane of symmetry. These flows consist of prominent regions of attachment bounded by streamwise separation lines which are shedding vortex sheets. Four trailing vortices are produced as a result of these separations. An accurate anatomy and origin of these separations is not understood at present.

The third important region of separation occurs at high angles of attack where the nacelle fore-body may separate and shed vorticity along the dorsal surface. These separation lines continue along the wing chord at low angles of attack, and begin to form the main vortex system which, at higher lift coefficients, keep the flow attached on the centre section and delays stall.

A leading edge extension, placed on the top of the nacelle at the wing leading edge modified the flow considerably. With this device fitted, the junction vortex, instead of being formed abruptly in the stagnation region between the wing and the nacelle, is now encouraged to separate more gradually along the streamwise edge of the LEX. The vortex sheet rolls up above the wing, producing downwash along the centreline, and increased lift. The separation lines which had originated on the edges of the nacelle continue across the chord to the trailing edge. The surface flow between them is not unlike that of a slender delta wing.

The effects of a propulsive flow on the wing-nacelle vortex characteristics were investigated by a flow survey using five-hole probes. This survey showed that the propeller slipstream was grossly deformed by the mutual effects of the wing and nacelle, and that as a result of separations in the wing-body junction, and roll up of the propeller streamtube, regions of concentrated vorticity were present in the flow.

REFERENCES

1. Smelt, R. et al — The Installation of an Engine Nacelle on a Wing, ARC R&M 2406, 1950.

2. Owen, E.
    Warden, R.
    Parkhurst, R.C. — Note on Wing-Nacelle Airscrew Interference. ARC R&M 2439, 1950.

3. Hoerner, S. — Aerodynamic Drag.

4. House, R.O.
    Wallace, A.R. — Wind Tunnel Investigation of the Effect of Interference on Lateral Stability Characteristics, etc. NACA Report 704, 1941.

5. Schlichting, H. — Report on the Special Field "Interference" to the Wind Tunnel Committee in February 1945, NACA TM 1347, May 1953.

6. Sandahl, C.
    Vollo, S. — Wind Tunnel Investigation of the Air Load Distribution on Two Combinations of Lifting Surfaces and Fuselage, NACA TN 1295, May 1947.

7. Wickens, R.H. — Observations of the Viscous Three-Dimensional Separations on Unpowered High-Wing Propeller Turbine Nacelle Models, NRC, NAE LTR-LA-258, February 1982.

8. McLellan, C.
    Cangelosi, J. — Effects of Nacelle Position on Wing-Nacelle Interference. NACA TN 1593, June 1948.

9. Becker, J.
    Leonard, L. — High-Speed Tests of a Model Twin-Engine Low Wing Transport Airplane, NACA R750, 1942.

10. Neely, R.H.
    Fairbanks, R.W.
    Conner, D.W. — Effects of Wing and Nacelle Modifications on the Drag and Wake Characteristics of a Bomber-Type Airplane Model, NACA ARR L5J05.

11. Johnston, F.
    Flawans, B.
    Danforth, E. — Flight Investigations of Factors Affecting the Carburetor Ram and Nacelle Drag of an A-26 Airplane, NACA MR L6F21.

12. Kayten, G.
    Koven, W. — Comparison of Wind-Tunnel and Flight Measurements fo Stability and Central Characteristics of a Douglas A-26 Airplane, NACA ARR L5I11a, March 1946.

13. Ashworth, C. — Pressure Distribution Measurements on Various Surfaces of a 0.2375-scale Model of the Douglas XA-26 Airplane in the 9-Foot Pressure Tunnel, NACA MR 90, October 1943.

14. Pepper, P. — Minimum Induced Drag in Wing-Fuselage Interference, NACA TN 812, September 1941.

15. Kuchemann, D. — Aerodynamic Design of Aircraft, Pergamon, 1978.

16. Weber, J — Interference Problems on Wing-Fuselage Combinations, Part I — Lifting Unswept Wing Attached to Cylindrical Fuselage at Zero Incidence in Mid-Wing Position, ARC CP 1331.

17. Weber, J.
    Joyce, M. — Interference Problems on Wing-Fuselage Combinations, Part II — Symmetrical Unswept Wing at Zero Incidence Attached to a Cylindrical Fuselage at Zero Incidence in Mid-Wing Position, ARC CP 1332.

18. Templin, R.J. — A Momentum Rule for Aircraft Performance in the V STOL Transition Regime, NRC, LR-470, January 1967.

19. Peake, D.J.
    Tobak, M. — Three-Dimensional Interactions and Vortical Flows with Emphasis on High Speeds, AGARD AG 252.

20. Maskell, E.C.   Flow Separation in Three Dimensions, Report Aero 2565, November 1955.

21. Young, A.D.   Some Special Boundary Layer Problems, 20th Ludwig Prandtl Memorial Lecture, May 1977, ZFW
                         Band 1, Heft 6, November 1977.

22. Wickens, R.H.   The Aerodynamic Characteristics and Trailing Vortex Wake of Propeller V/STOL Configurations,
                         Canadian Aeronautics and Space Institute Journal, Vol. 21, No. 3, March 1975.
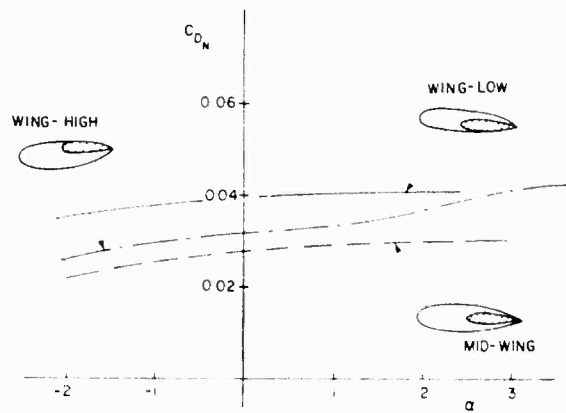
FIG 1   EFFECT OF NACELLE VERTICAL POSITION ON NACELLE DRAG (REF 9)
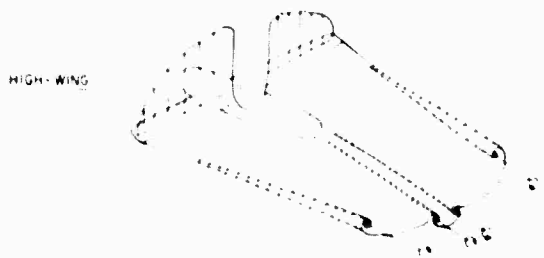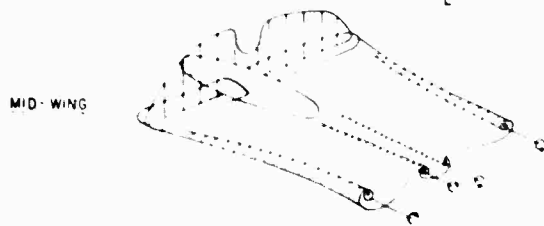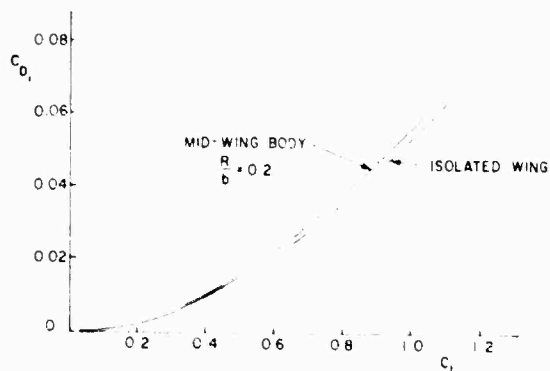
INDUCED DRAG AND LIFT DISTRIBUTION FOR WING BODY CONFIGURATIONS
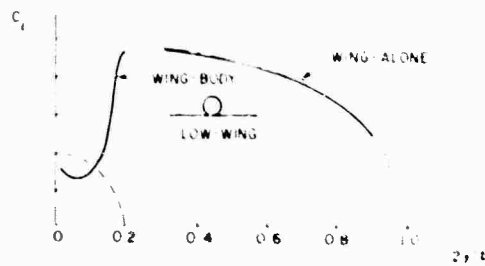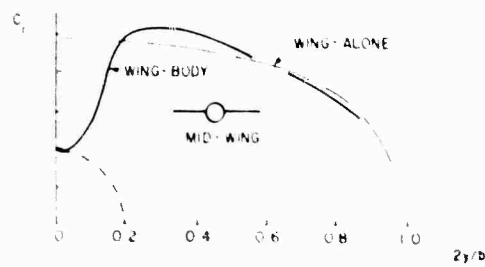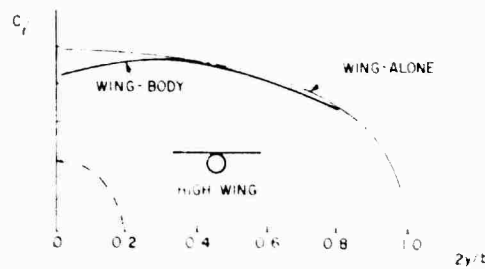
FIG 4   SPANWISE LOAD DISTRIBUTIONS OF WING BODY CONFIGURATIONS

FIG. 2: TURBULENT SEPARATION IN EXPANDING CORNER — UNDERSLUNG NACELLES

FIG. 5: ISOBARS ON WING UPPER SURFACE OF HIGH-WING MODEL, SHOWING SUCTION CONCENTRATION
AT THE WING ROOT JUNCTION $\alpha = 2.5°$, M = 0.6 (REF. 8)
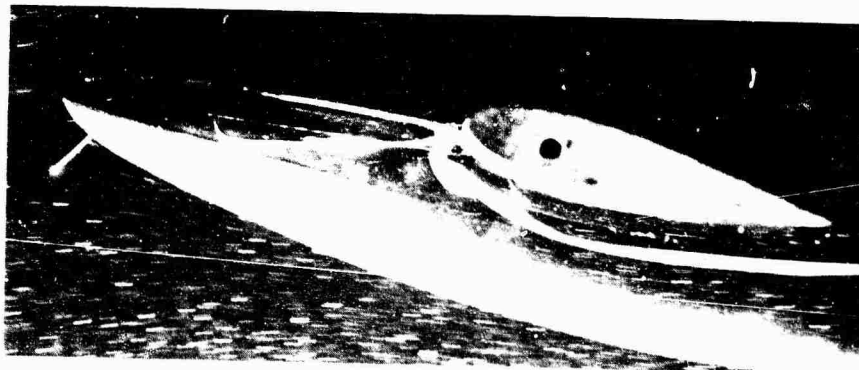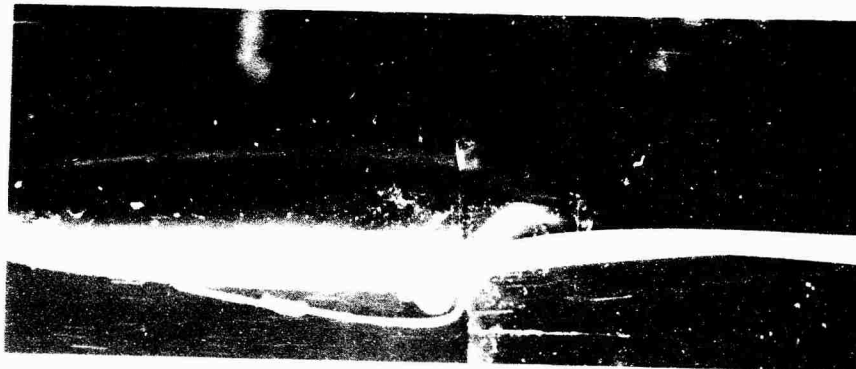
FIG. 6: VORTEX FLOWS IN THE WING ROOT JUNCTION
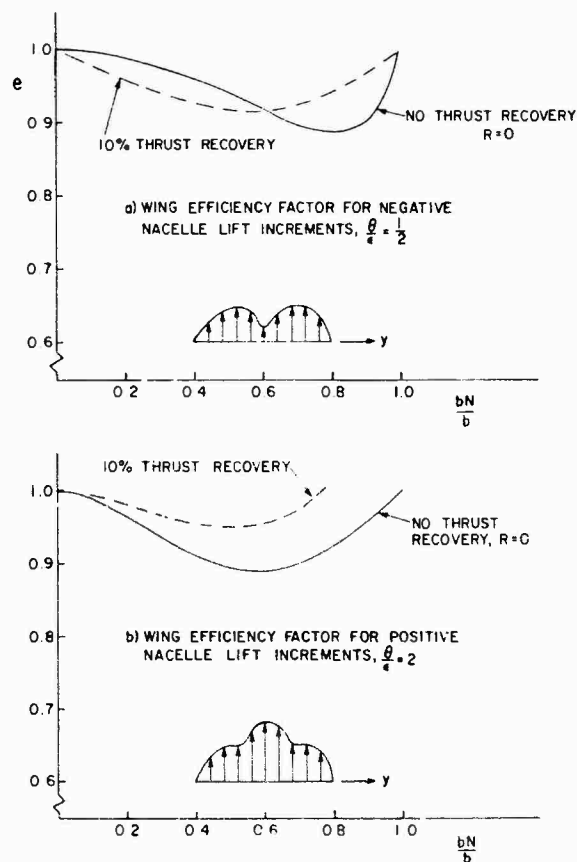
FIG. 7: WING EFFICIENCY FACTOR FOR POWERED LIFT AIRCRAFT
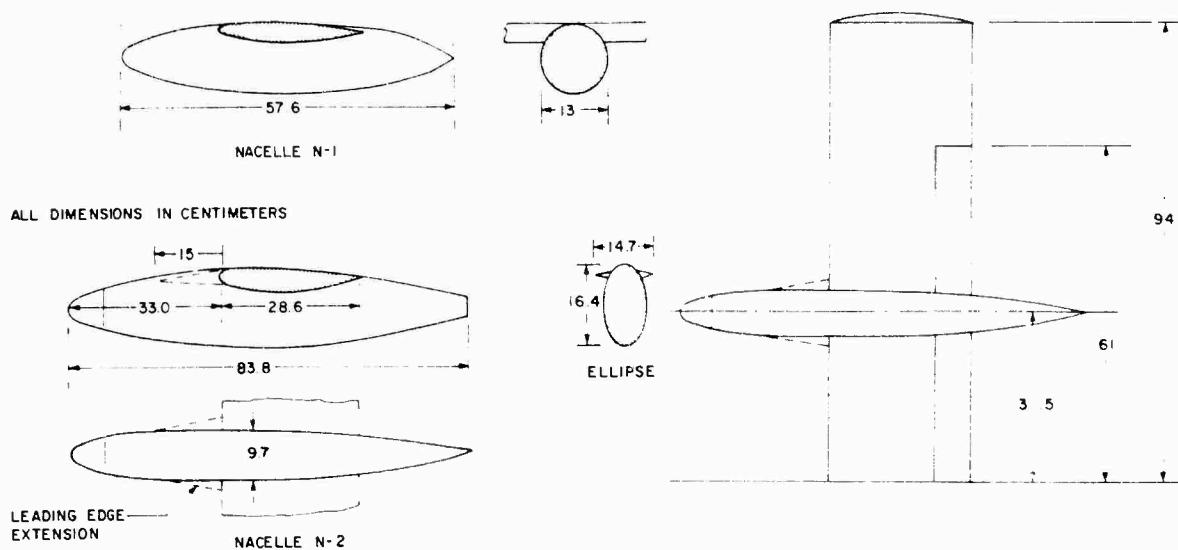
FIG. 8: GENERAL ARRANGEMENT OF HALF-MODEL CONFIGURATION
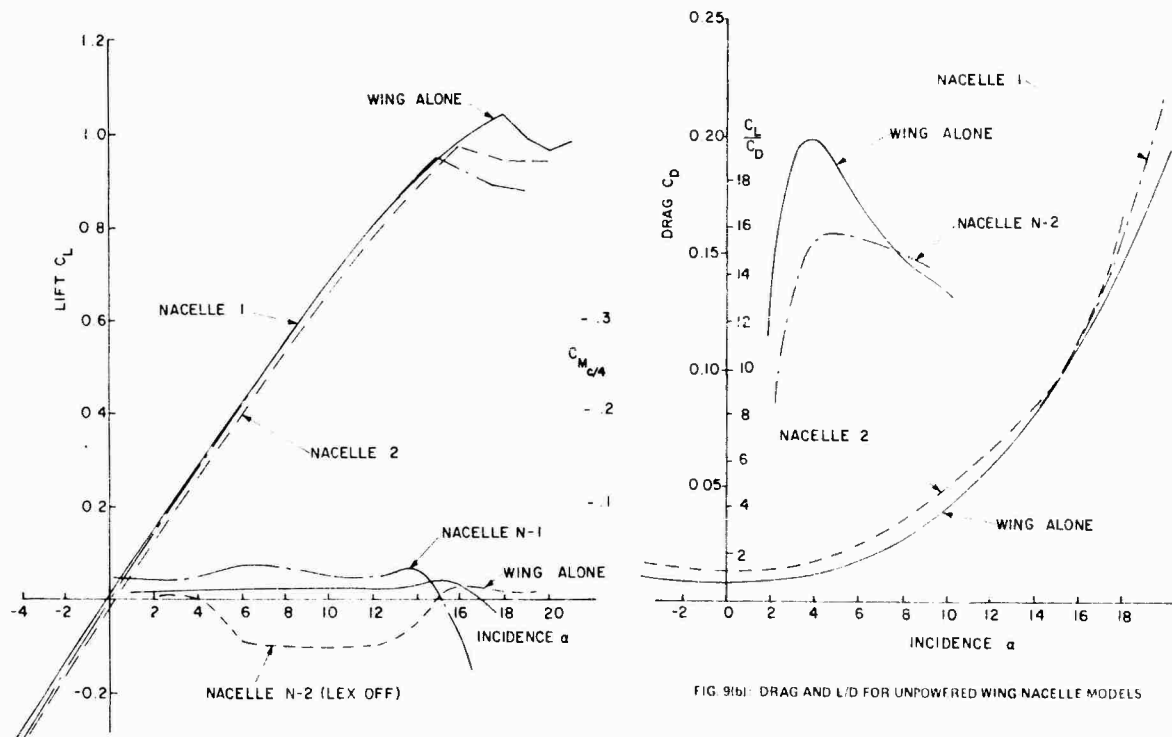
FIG. 9(a): LIFT AND MOMENT CHARACTERISTICS UNPOWERED WING NACELLE MODELS

FIG. 9(b): DRAG AND L/D FOR UNPOWERED WING NACELLE MODELS

FIG. 9   LIFT AND MOMENT CHARACTERISTICS UNPOWERED WING-NACELLE MODELS
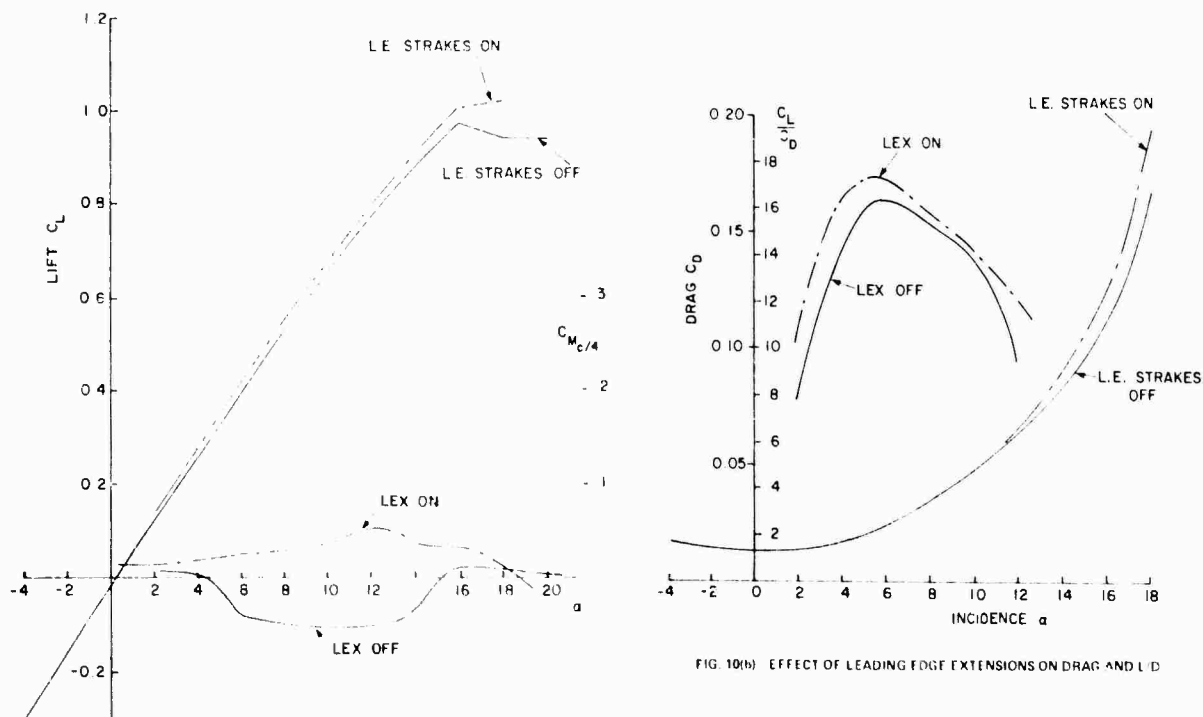
FIG. 10(a): EFFECT OF LEADING EDGE EXTENSIONS ON LIFT AND MOMENT — NACELLE 2

FIG. 10(b) EFFECT OF LEADING EDGE EXTENSIONS ON DRAG AND L/D

FIG. 10   EFFECT OF LEADING EDGE EXTENSIONS ON LIFT AND MOMENT — NACELLE 2

a) NODAL POINT OF ATTACHMENT - WINDWARD SIDE
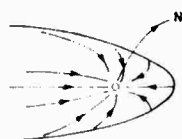
b) SEPARATION FROM LEE SIDE

c) OBLIQUE LINE OF ATTACHMENT ON WINDWARD SURFACE
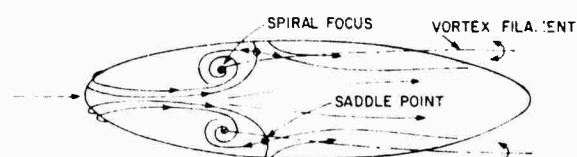
d) SEPARATION FROM SPIRAL FOCI
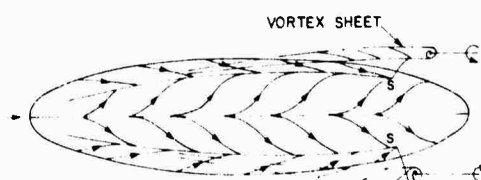
e) OBLIQUE LINES OF SEPARATION ON LEEWARD SURFACE

FIG. 11: CLASSIFICATION OF VISCOUS FLOWS
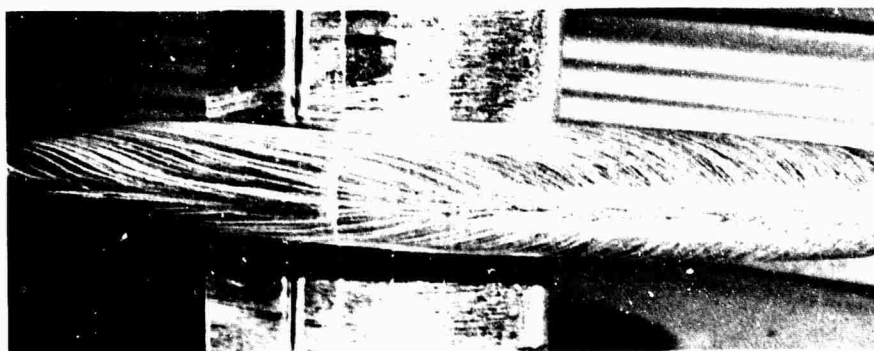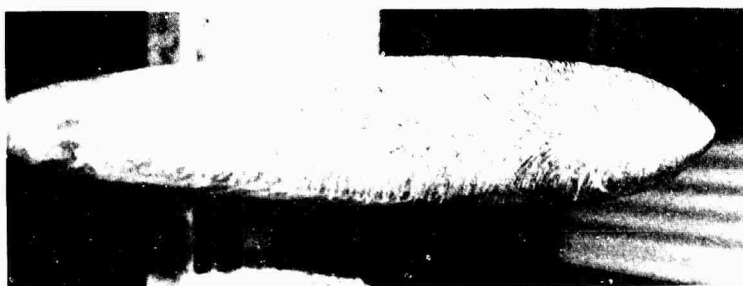
FIG. 12: ATTACHMENT FLOWS ON NACELLE N-2 FOREBODY — $\alpha = 20°$
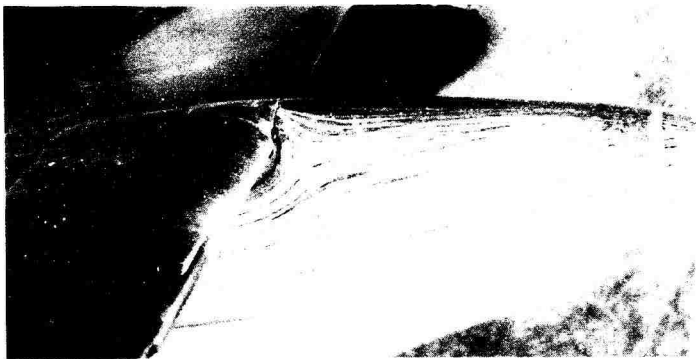
a) N-2 $\alpha = 0$

b) N-2 $\alpha = 8°$
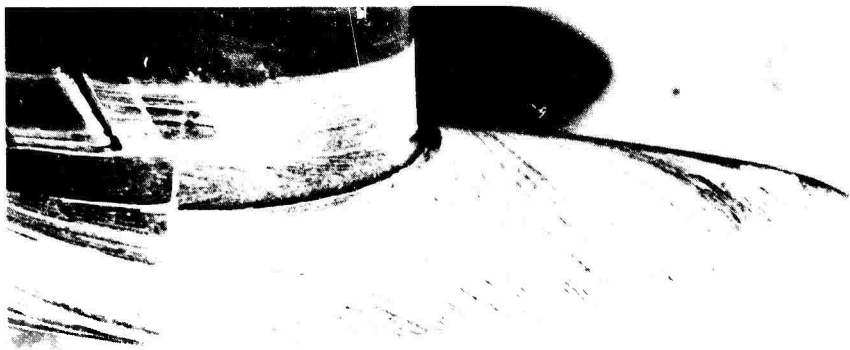
c) N-2 $\alpha = 16°$
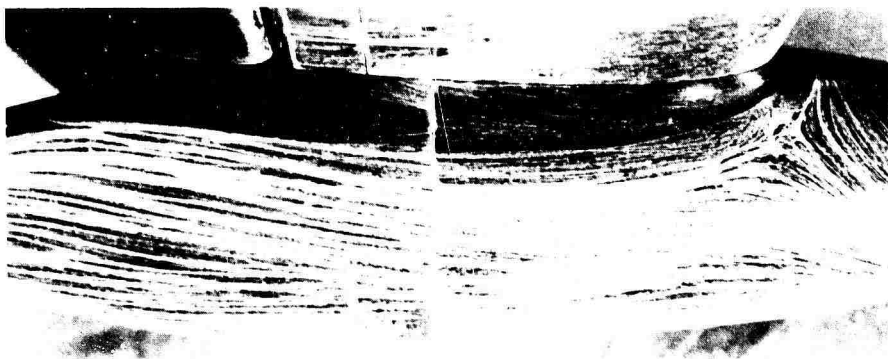
d) N-1 $\alpha = 16°$

FIG. 13: SEPARATION AND ATTACHMENT IN THE WING-ROOT JUNCTION — NO LEADING EDGE EXTENSION
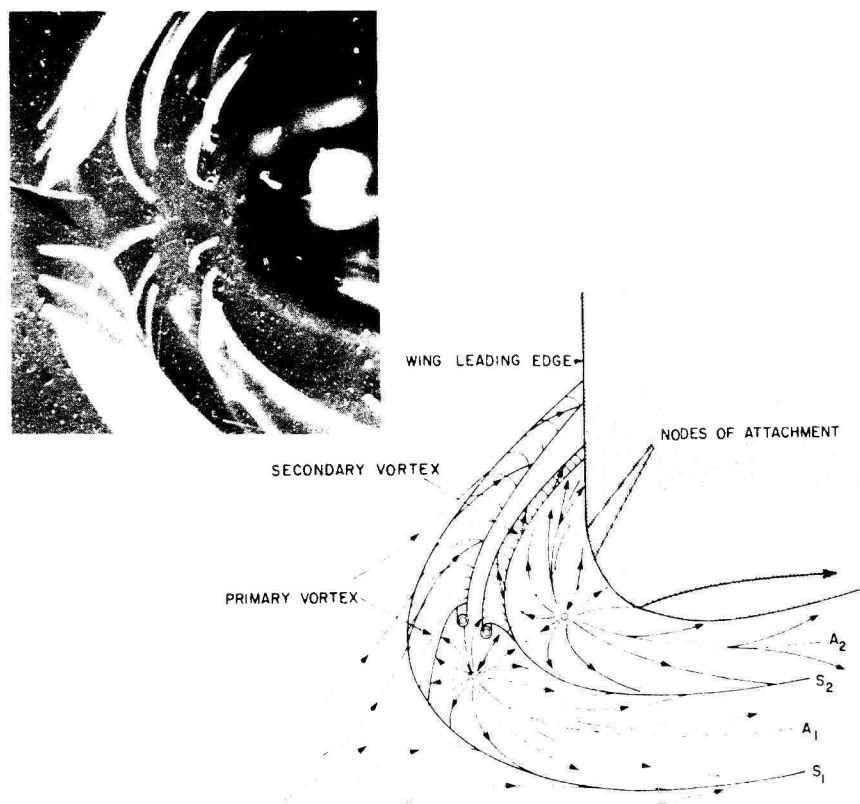
FIG. 14: FLOW IN THE WING-BODY JUNCTION — NO LEADING EDGE EXTENSION
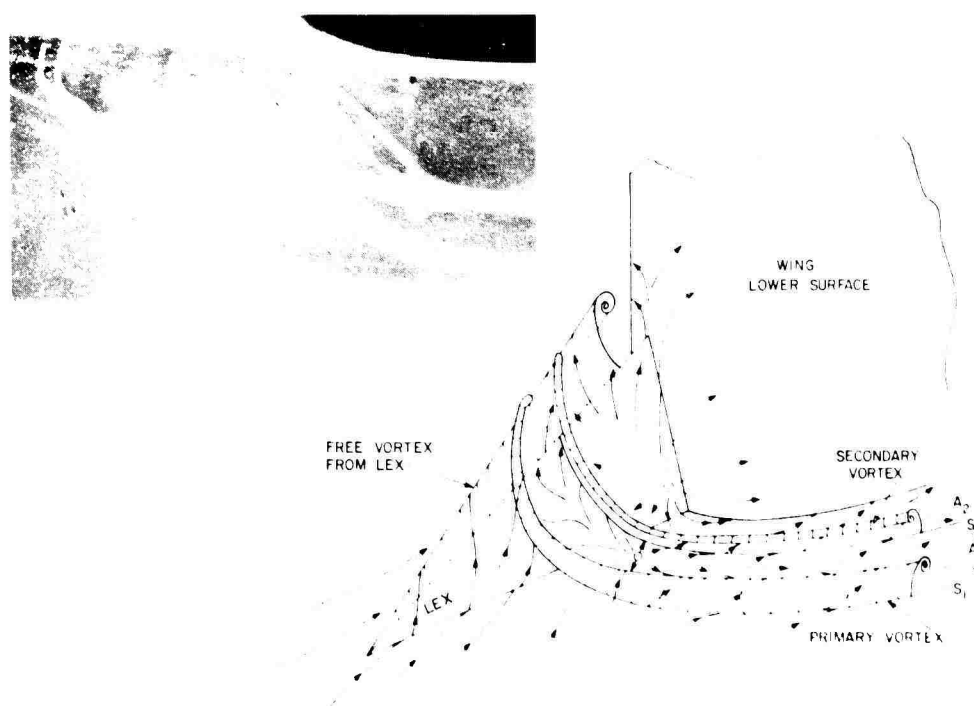
FIG. 16: VISCOUS VORTEX SEPARATION ON WINDWARD SURFACE OF LEADING EDGE EXTENSION
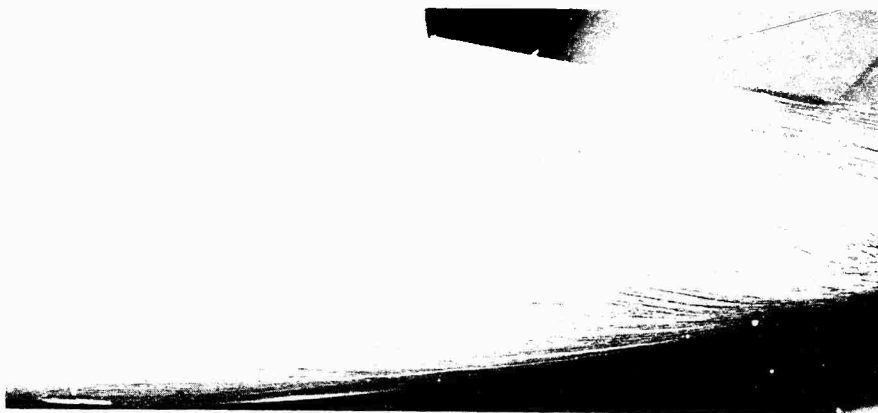
a) N-2 $\alpha = 8°$

b) N-2 $\alpha = 8°$

c) N-2 $\alpha = 16°$

FIG. 15: SEPARATION AND ATTACHMENT IN THE WING-ROOT JUNCTION – WITH LEADING EDGE EXTENSION
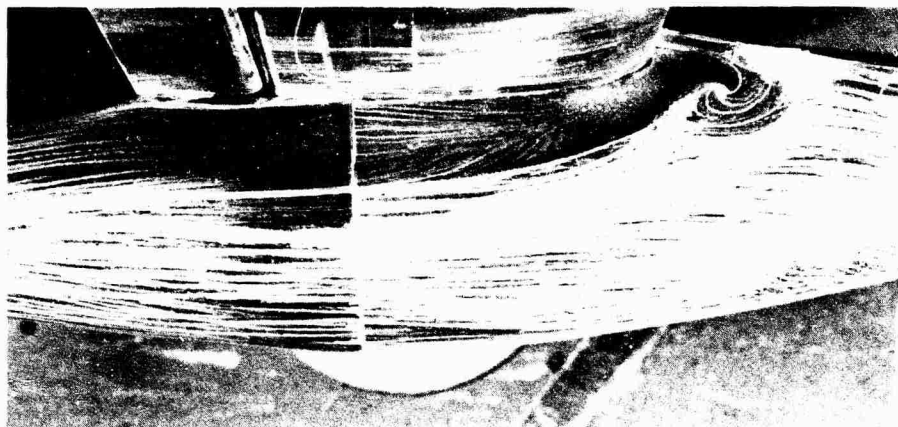
FIG. 17(a): UNDER-WING VORTEX SHED FROM SPIRAL FOCUS IN WING-ROOT JUNCTION
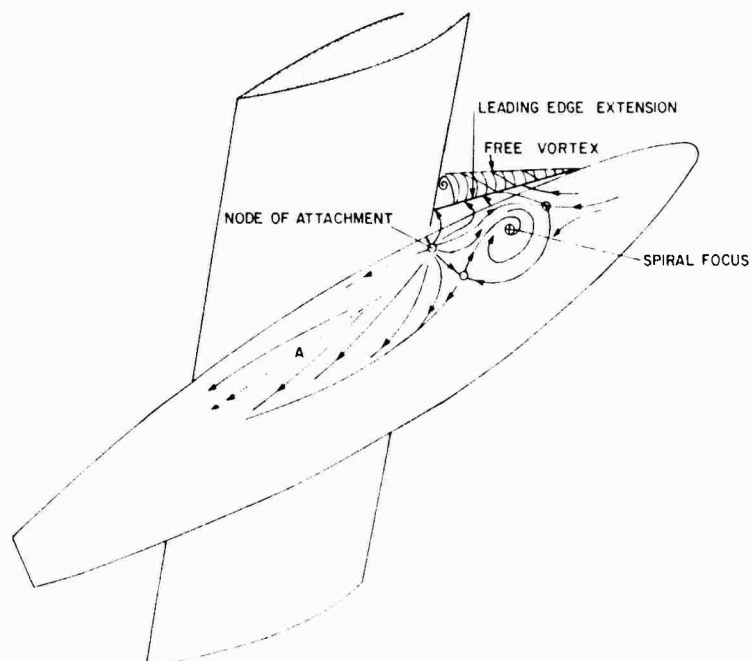
FIG. 17(b): JUNCTION FLOW WITH LEADING EDGE EXTENSION — VORTEX FILAMENT
ISSUING FROM SPIRAL FOCUS

FIG. 18(a): FLOW ON NACELLE UPPER SURFACE — NO LEADING EDGE EXTENSION,
NACELLE N-1, $\alpha = 16^\circ$

VORTEX SHEETS DEVELOPING
ON NACELLE UPPER SURFACE
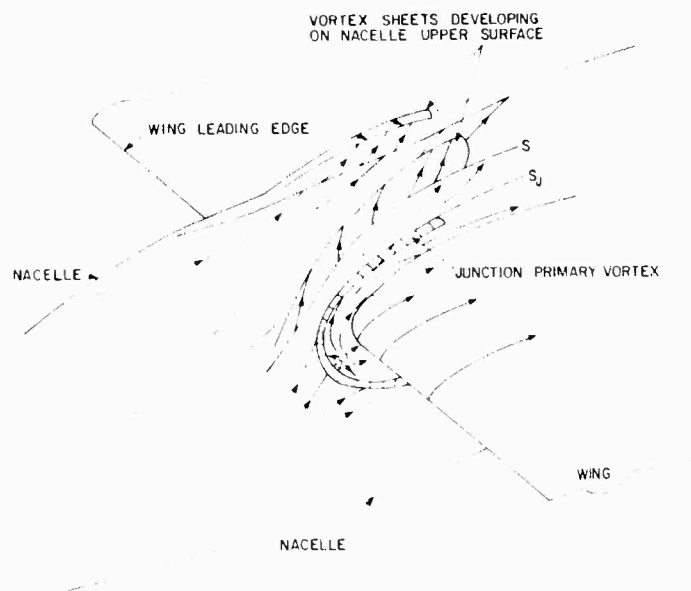
FIG. 18(b): DEVELOPMENT OF THREE-DIMENSIONAL VORTEX SHEETS ON NACELLE UPPER SURFACE
AT ANGLES BELOW STALL — NO LEADING EDGE EXTENSION
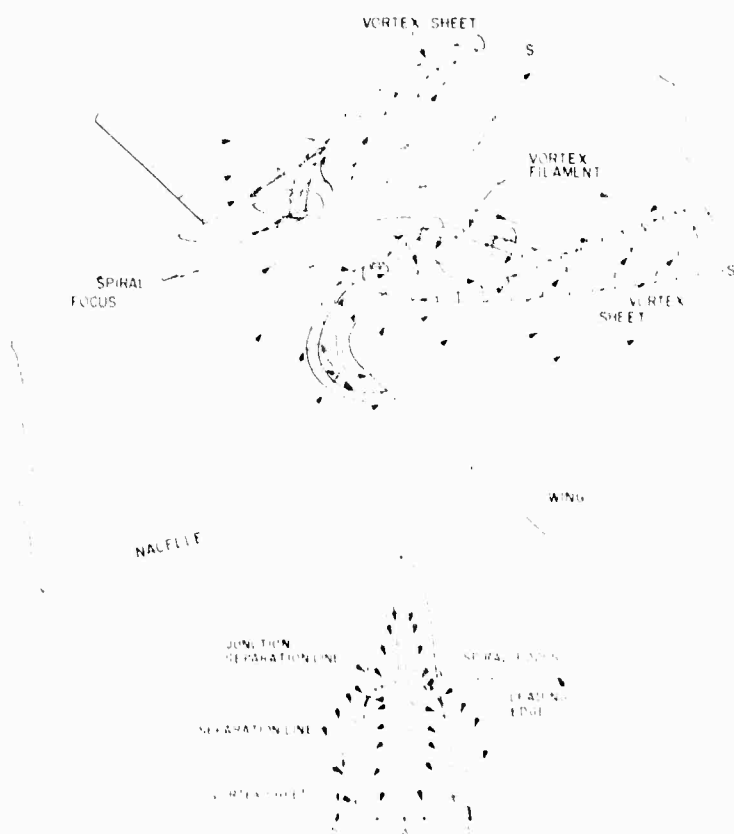
FIG. 20: DEVELOPMENT OF WING UPPER SURFACE VORTEX FLOWS — NO LEADING EDGE EXTENSION
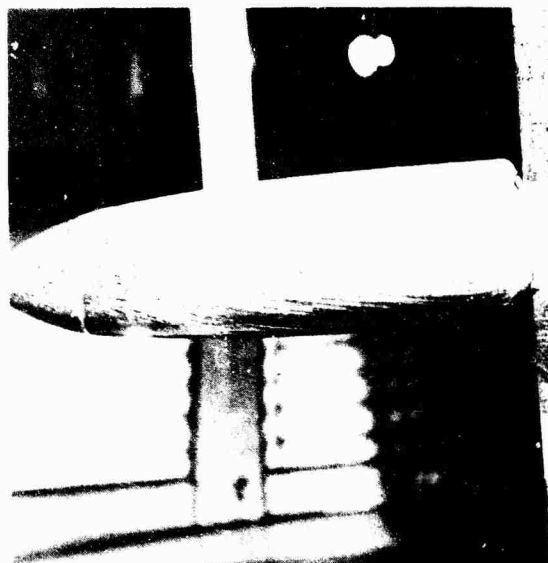
a) $\alpha = 0°$
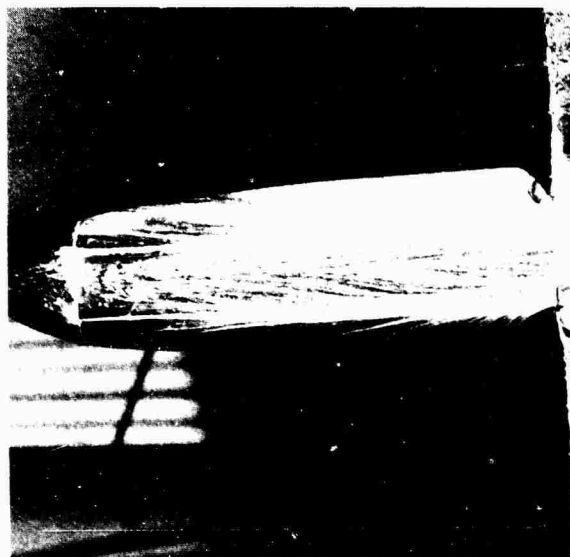
b) $\alpha = 20°$

c) $\alpha = 16°$

FIG. 19 WING UPPER SURFACE FLOW   NO LEADING EDGE EXTENSION

a) α = O   NACELLE N-2

b) α = 8°   NACELLE N-2

c) α = 16° NACELLE N-2

FIG. 21: FLOW ON THE WING UPPER SURFACE — LEADING EDGE EXTENSION ON
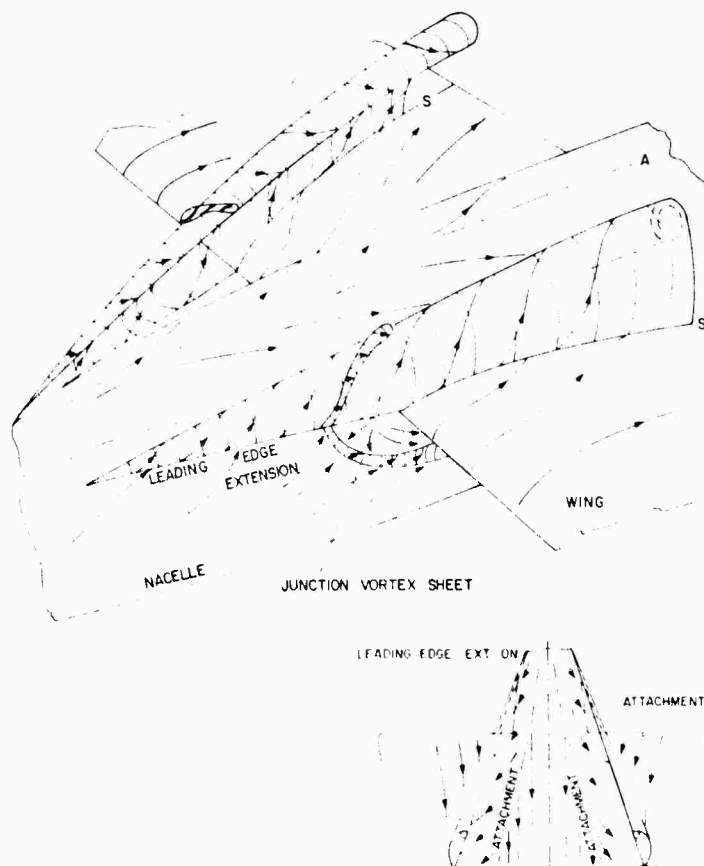
FIG. 22: DEVELOPMENT OF WING UPPER SURFACE VORTEX FLOWS

LEADING EDGE EXTENSION ON
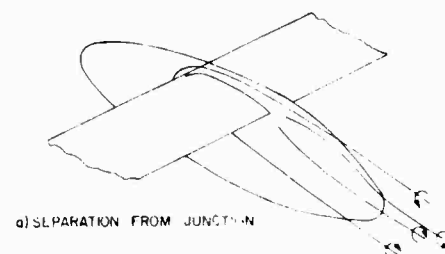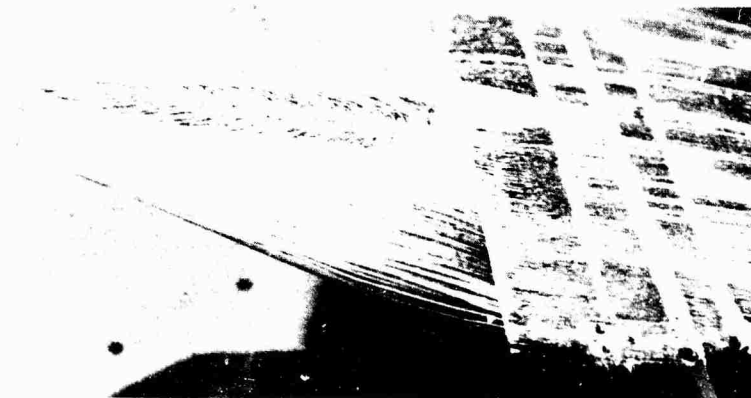

a) SEPARATION FROM JUNCTION
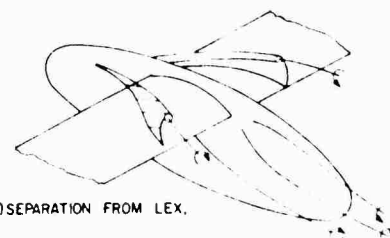
b) SEPARATION FROM LEX.
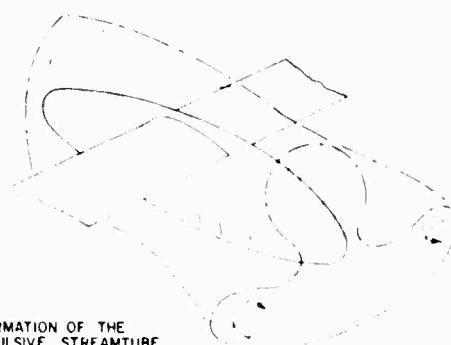
c) DEFORMATION OF THE PROPULSIVE STREAMTUBE

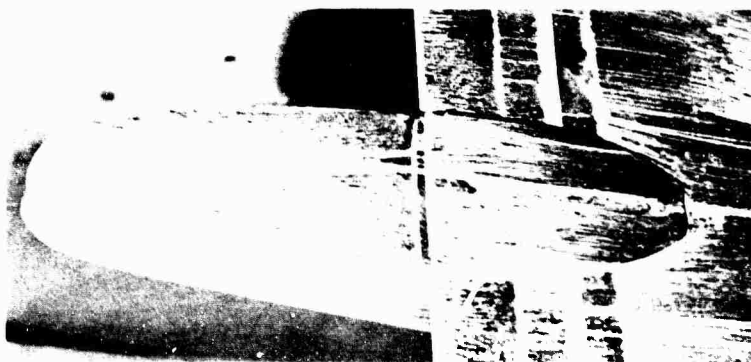FIG. 26: WAKE-VORTEX SYSTEMS FOR WING-NACELLE CONFIGURATIONS

FIG. 23: DETACHMENT OF WING VORTEX SHEETS WITH FORMATION OF DOUBLE-BRANCHED CORES — LEADING EDGE EXTENSION ON
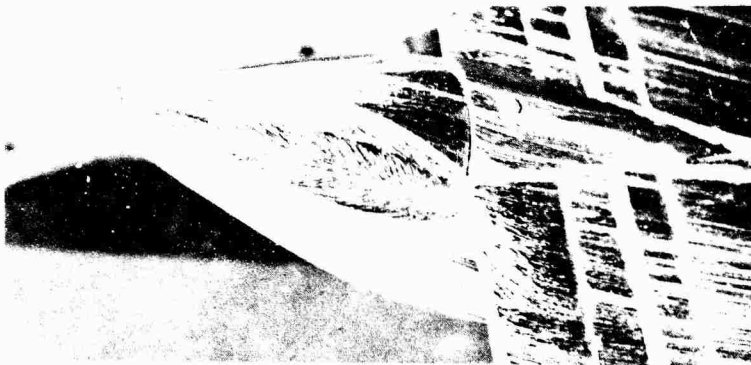
a) NACELLE N-1 $\alpha = 8°$

b) NACELLE N-2 $\alpha = 0°$

c) SEPARATION FROM

LINE OF CONFLUENCE $\alpha = 0°$

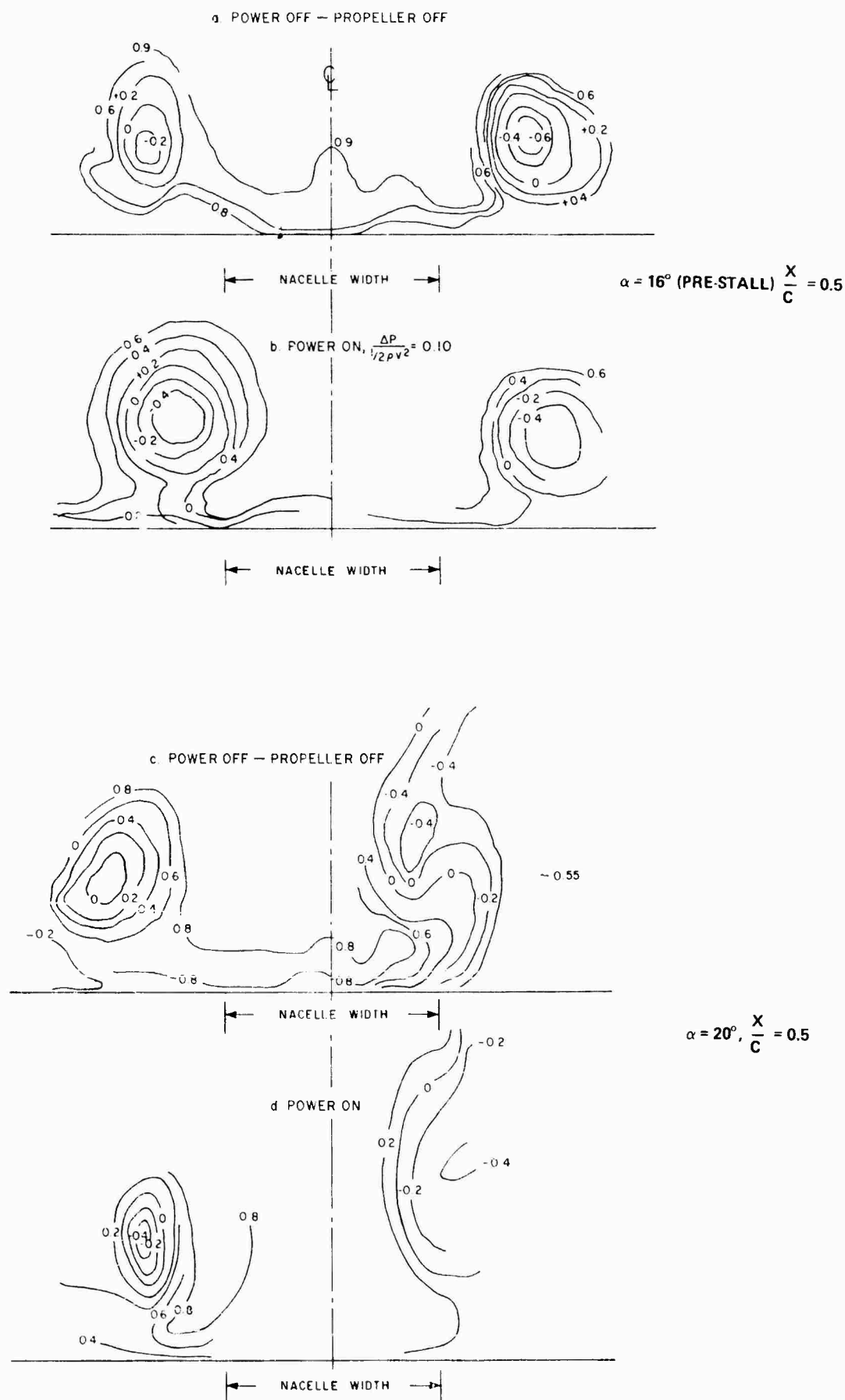FIG. 24   SEPARATION AND ATTACHMENT FROM NACELLE AFTERBODIES

a. POWER OFF — PROPELLER OFF

$\alpha = 16°$ (PRE-STALL) $\frac{X}{C} = 0.5$

b. POWER ON, $\frac{\Delta P}{\frac{1}{2}\rho V^2} = 0.10$

c. POWER OFF — PROPELLER OFF

$\alpha = 20°$, $\frac{X}{C} = 0.5$

d. POWER ON

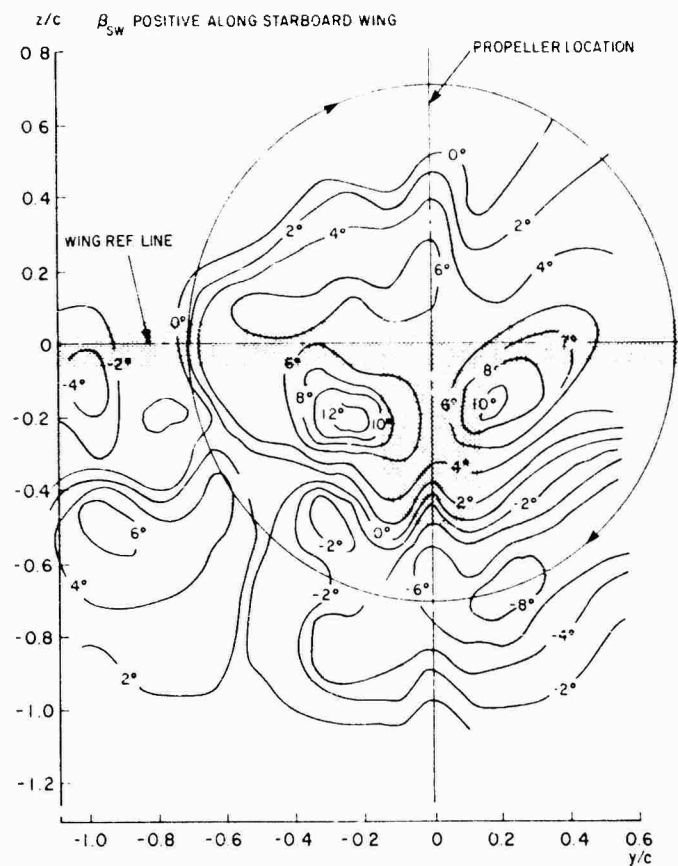FIG. 27: TOTAL PRESSURE SURVEY Cp_T ON WING UPPER SURFACE NACELLE N-2 (LEX ON)

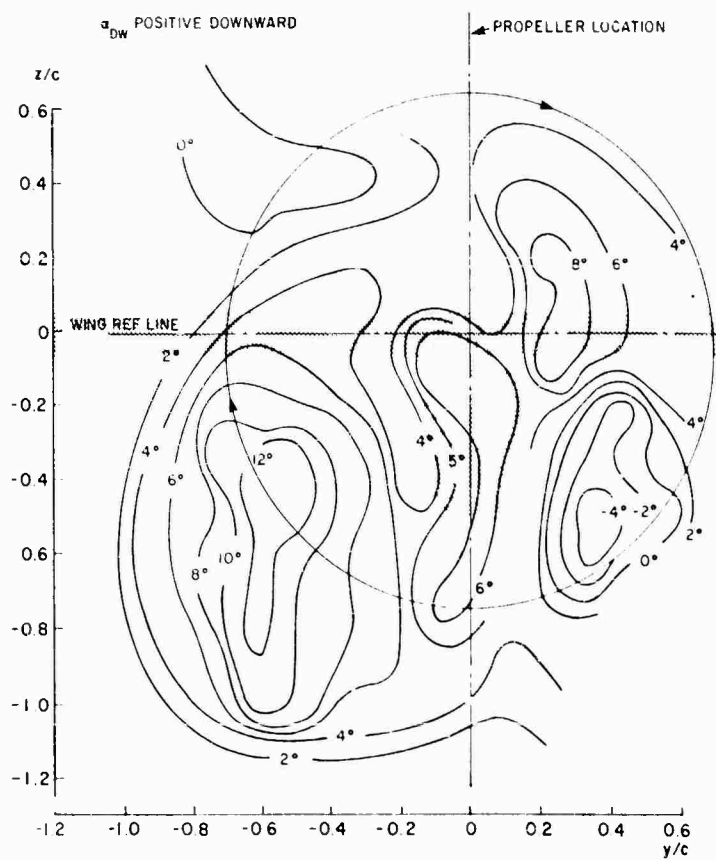FIG. 28(a): SIDEWASH ANGLE DOWNWIND OF QUASI-2-D POWERED WING-NACELLE MODEL

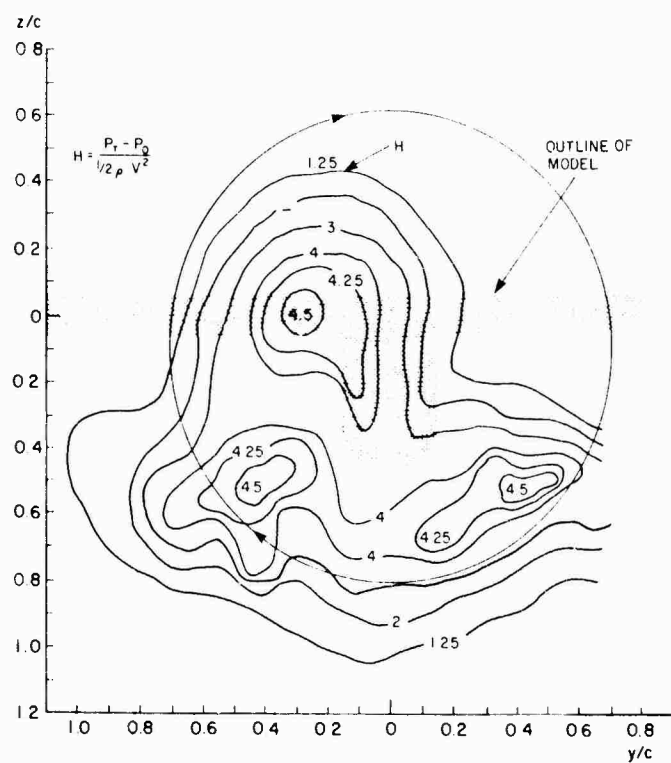FIG. 28(b): DOWNWASH ANGLE DOWNWIND OF QUASI-2-D POWERED WING-NACELLE MODEL

$$H = \frac{P_T - P_0}{1/2 \rho \, V^2}$$

FIG. 29: TOTAL PRESSURE H, DOWNWIND OF QUASI-2-D POWERED WING-NACELLE MODEL